ligase activates the anaphase promoting complex to allow progression beyond prometaphase. *Dev. Cell* **4**, 813-826.

Melixetian, M., Klein, D. K., Sorensen, C. S. and Helin, K. (2009). NEK11 regulates CDC25A degradation and the IR-induced G2/M checkpoint. *Nat. Cell Biol.* **11**, 1247-1253.

Miyata, H., Doki, Y., Yamamoto, H., Kishi, K., Takemoto, H., Fujiwara, Y., Yasuda, T., Yano, M., Inoue, M., Shiozaki, H. et al. (2001). Overexpression of CDC25B overrides radiation-induced G2-M arrest and results in increased apoptosis in esophageal cancer cells. *Cancer Res.* **61**, 3188-3193.

Morgan, D. O. (1995). Principles of CDK regulation. *Nature* **374**, 131-134.

Ray, D., Terao, Y., Nimbalkar, D., Hirai, H., Osmundson, E. C., Zou, X., Franks, R., Christov, K. and Kiyokawa, H. (2007). Hemizygous disruption of Cdc25A inhibits cellular transformation and mammary tumorigenesis in mice. *Cancer Res.* **67**, 6605-6611.

Seki, A., Coppinger, J. A., Du, H., Jang, C. Y., Yates, J. R., 3rd and Fang, G. (2008). Plk1- and beta-TrCP-dependent degradation of Bora controls mitotic progression. *J. Cell Biol.* **181**, 65-78.

Uchida, S., Kuma, A., Ohtsubo, M., Shimura, M., Hirata, M., Nakagama, H., Matsunaga, T., Ishizaka, Y. and Yamashita, K. (2004). Binding of 14-3-3beta but not 14-3-3sigma controls the cytoplasmic localization of CDC25B: binding site preferences of 14-3-3 subtypes and the subcellular localization of CDC25B. *J. Cell Sci.* **117**, 3011-3020.

Uchida, S., Yoshioka, K., Kizu, R., Nakagama, H., Matsunaga, T., Ishizaka, Y., Poon, R. Y. and Yamashita, K. (2009). Stress-activated mitogen-activated protein kinases c-Jun NH2-terminal kinase and p38 target Cdc25B for degradation. *Cancer Res.* **69**, 6438-6444.

Watanabe, N., Arai, H., Nishihara, Y., Taniguchi, M., Hunter, T. and Osada, H. (2004). M-phase kinases induce phospho-dependent ubiquitination of somatic Wee1 by SCF$^{beta\text{-}TrCP}$. *Proc. Natl. Acad. Sci. USA* **101**, 4419-4424.

Westbrook, T. F., Hu, G., Ang, X. L., Mulligan, P., Pavlova, N. N., Liang, A., Leng, Y., Maehr, R., Shi, Y., Harper, J. W. et al. (2008). SCF$^{beta\text{-}TrCP}$ controls oncogenic transformation and neural differentiation through REST degradation. *Nature* **452**, 370-374.

Winston, J. T., Strack, P., Beer-Romero, P., Chu, C. Y., Elledge, S. J. and Harper, J. W. (1999). The SCF$^{beta\text{-}TrCP}$-ubiquitin ligase complex associates specifically with phosphorylated destruction motifs in IκBα and β-catenin and stimulates IκBα ubiquitination *in vitro*. *Genes Dev.* **13**, 270-283.

Wu, G., Xu, G., Schulman, B. A., Jeffrey, P. D., Harper, J. W. and Pavletich, N. P. (2003). Structure of a beta-TrCP1-Skp1-beta-catenin complex: destruction motif binding and lysine specificity of the SCF$^{beta\text{-}TrCP1}$ ubiquitin ligase. *Mol. Cell* **11**, 1445-1456.

Yao, Y., Slosberg, E. D., Wang, L., Hibshoosh, H., Zhang, Y. J., Xing, W. Q., Santella, R. M. and Weinstein, I. B. (1999). Increased susceptibility to carcinogen-induced mammary tumors in MMTV-Cdc25B transgenic mice. *Oncogene* **18**, 5159-5166.

Journal of Cell Science

Radiosensitization effect of poly(ADP-ribose) polymerase inhibition in cells exposed to low and high liner energy transfer radiation

Takahisa Hirai,[1,2] Hidenori Shirai,[1] Hiroaki Fujimori,[1] Ryuichi Okayasu,[3] Keisuke Sasai[2] and Mitsuko Masutani[1,4]

[1]Division of Genome Stability Research, National Cancer Center Research Institute, Tokyo, Japan; [2]Department of Radiology, Juntendo University Graduate School of Medicine, Tokyo, Japan; [3]International Open Laboratory, National Institute of Radiological Sciences, Chiba, Japan

(Received December 13, 2011/Revised February 19, 2012/Accepted February 26, 2012/Accepted manuscript online March 10, 2012)

Poly(ADP-ribose) polymerase (PARP)-1 promotes base excision repair and DNA strand break repair. Inhibitors of PARP enhance the cytotoxic effects of γ-irradiation and X-irradiation. We investigated the impact of PARP inhibition on the responses to γ-irradiation (low liner energy transfer [LET] radiation) and carbon-ion irradiation (high LET radiation) in the human pancreatic cancer cell line MIA PaCa-2. Cell survival was assessed by colony formation assay after combination treatment with the PARP inhibitor AZD2281 and single fraction γ-irradiation and carbon-ion irradiation (13 and 70 keV/μm [LET 13 and LET 70]). The DNA damage response (DDR) was assessed by pulse field gel electrophoresis, western blotting and flow cytometry. Treatment with a PARP inhibitor enhanced the cytotoxic effect of γ-irradiation and LET 13 and LET 70 carbon-ion irradiation. Moreover, the radiosensitization effect was greater for LET 70 than for LET 13 irradiation. Prolonged and increased levels of γ-H2AX were observed both after γ-irradiation and carbon-ion irradiation in the presence of the PARP inhibitor. Enhanced level of phosphorylated-p53 (Ser-15) was observed after γ-irradiation but not after carbon-ion irradiation. PARP inhibitor treatment induced S phase arrest and enhanced subsequent G2/M arrest both after γ-irradiation and carbon-ion irradiation. These results suggest that the induction of S phase arrest through an enhanced DDR and a local delay in DNA double strand break processing by PARP inhibition caused sensitization to γ-irradiation and carbon-ion irradiation. Taken together, PARP inhibitors might be applicable to a wide therapeutic range of LET radiation through their effects on the DDR. (*Cancer Sci*, doi: 10.1111/j.1349-7006.2012.02268.x, 2012)

A definite cell-killing effect with minimal adverse events during the lifetime of patients is among the main goals of radiotherapy for cancer treatment. To achieve this goal, both the improvement of dose distribution and the development of efficient radiosensitizers are important.

In addition to conventional photons, such as X-rays and γ-rays, other types of radiation, such as high liner energy transfer (LET) charged particles and protons, are being used in cancer therapy with good clinical outcomes.[1] Carbon-ion radiation has significant biological advantages compared with photon beams,[2] and radiosensitizers should result in further improvement of the effectiveness of carbon-ion radiation therapy. However, effective radiosensitizers for high LET radiation are not currently available.

In the search for chemotherapeutic agents, recent interest has focused on DNA repair pathways as potential targets for novel cancer treatments.[3] The poly(ADP-ribose) polymerase (PARP) superfamily consists of 17 members, which are multifunctional enzymes, and PARP-1 is the most abundant. PARP-1 detects the presence of DNA single and double strand breaks (SSB and DSB) and binds to the sites of damage, promoting DNA repair by modifying key proteins.[4] PARP-1 is upregulated in various cancers, presumably to compensate for genomic instability,[5] making this enzyme a target of cancer therapy. PARP inhibitors cause synthetic lethality in cells with mutations in *BRCA1* or *BRCA2*, which encode important proteins for homologous recombination (HR)[6] or in HR-deficient cancer cells. In fact, clinical studies suggest that PARP inhibitors are effective as mono-therapy against *BRCA*-mutated cancers, showing few adverse effects compared with conventional chemotherapy,[7] and PARP inhibitor treatment in combination with conventional chemotherapy improves survival of cancer patients without increasing toxic effects.[8,9] PARP inhibitors also enhance the cytotoxicity of ionizing radiation in various cancer cells and animal models.[10–12] Because PARP-1 is an important enzyme for base excision repair (BER)[13] and radiation-induced SSB are mainly repaired by BER, the radiosensitization effect of PARP inhibitors is thought to occur through a block in the BER pathway, leading to an increase of collapsed replication forks generating persistent DSB, which are potentially lethal lesions.[14] Dungey *et al.*[10] demonstrate that the radiosensitizing effects of PARP inhibitors on photon beams are S phase-dependent.

Because biological enhancement of high LET radiation might contribute to the development of more effective cancer therapies, we investigated the effect of PARP inhibition on the responses to γ-irradiation (low LET radiation) as well as carbon-ion irradiation (high LET radiation).

Materials and Methods

Chemicals and antibodies. AZD2281 (Olaparib) was obtained from Selleck Chemicals (Houston, TX, USA) and dissolved in DMSO. Anti-γ-H2AX (Ser-139) antibody was purchased from Millipore (Billerica, MA, USA). Anti-phosphorylated p53 (Ser-15), and anti-histone H3 antibodies were obtained from Cell Signaling Technology (Danvers, MA, USA). Anti-phosphorylated histone H3 (Ser-10) antibody was purchased from Abcam (Cambridge, UK). Anti-β-actin was purchased from Sigma-Aldrich (St. Louis, MO, USA).

Cell culture. The human pancreatic cancer cell line MIA PaCa-2 was obtained from the American Type Culture Collection (Rockville, MD, USA) and maintained in DMEM supplemented with 10% FBS and 1% penicillin/streptomycin at 37°C in a humidified atmosphere containing 5% CO_2 and 95% air.

Irradiation. Exponentially growing cells were irradiated with γ-rays and carbon-ion beams. For γ-irradiation, ^{60}Co γ-irradiator (Gammacell 220, Nordion, Canada) was used at 0.29 Gy/sec at the National Cancer Center Research Institute. Carbon-ion

[4]To whom correspondence should be addressed.
E-mail: mmasutan@ncc.go.jp

doi: 10.1111/j.1349-7006.2012.02268.x

beams (290 MeV/n, 13 and 70 keV/μm) were generated by a heavy ion medical accelerator at the National Institute of Radiological Sciences (NIRS). LET 13 and LET 70 carbon-ion monobeams were used because they are the representative LET at the entrance region to which normal tissues adjacent to tumors are exposed and near at the Bragg peak to target tumor volume, respectively. Cells in flasks were placed in a specially designed rack for correct positioning. Irradiation was conducted using horizontal carbon-ion beams with a dose rate of approximately 1.2 Gy/min. The energy at the irradiation site was obtained by comparing the calculated and measured depth–dose distribution. The LET values (dose averaged LET) at the sample position were compensated with Lucite absorbers.

Clonogenic survival assays. Cells were seeded in triplicate in six-well tissue culture dishes with 3 mL of culture medium and in 25-cm^2 flasks with 5 mL of culture medium 10–14 h before γ-irradiation and carbon-ion beam (LET 13 and 70 keV/μm) irradiation, respectively. This 4-h interval was the time needed for seeding and irradiation. AZD2281 at 1 μM, 5 μM or 0.1% of DMSO (solvent control) were added to the medium 2–3 h before irradiation. Following irradiation, the cells were incubated at 37°C in a CO_2 incubator. After 5–6 days, surviving colonies were fixed with 4% formalin solution and stained with 0.02% crystal violet solution. In the literature, for colony formation assay, approximately 5 Gy is the usual maximum dose for carbon-ion irradiation.[15,16] Therefore, the cell survival and the sensitization effect of the chemicals were evaluated with 1–5 Gy of carbon-ion irradiation. Colonies composed of more than approximately 50 cells were counted. Cell survival was calculated by dividing the number of colonies of irradiated cells by the number of inoculated cells and plating efficiencies of the control cells in each condition. The result of γ-ray irradiation was calculated from the average of at least three independent experiments performed in triplicate. The average of nine data points was used to generate a survival curve. Standard deviation was calculated and statistical analysis was carried out. For carbon-ion irradiation, experiments were performed three times, and the representative result is shown. The plating efficiency of MIA PaCa-2 was 0.55 ± 0.15. To evaluate the radio-sensitizing effects of AZD2281, the ratio of radiation doses to give 10% cell survival for radiation alone and radiation plus AZD2281 was calculated.

Pulse field gel electrophoresis. Cells were trypsinized and 1.5×10^5 cells were embedded in 1% agarose (Bio-Rad, Hercules, CA, USA) and digested in a proteinase K buffer (0.5 M EDTA; 1% sodium N-lauroylsarcosine, 0.5 mg/mL proteinase K) at 50°C for 20 h, followed by washing in 50 mM EDTA (pH 8.0). Electrophoresis was performed for 20 h at 14°C in 1% pulse field-certified agarose (Bio-Rad) gels containing 0.5 × Tris-borate/EDTA buffer and adapted to a CHEF Mapper Pulse Field Electrophoresis System (Bio-Rad). Markers of λ phage DNA digested with Hind III were loaded. Gels were stained with ethidium bromide and analyzed with LAS 3000 (Fuji Film, Tokyo, Japan).

A modification of a Southern blot hybridization method that uses total human genomic DNA as a probe was used. Briefly, total human genomic DNA was labeled with [α-^{32}P] dCTP using the Megaprime DNA labeling System (GE Healthcare, Waukesha, WI, USA) and hybridization was carried out as described elsewhere[17] and analyzed by BAS 2500 (Fuji Film).

Western blot analysis. MIA PaCa-2 cells were extracted with Laemmli buffer, sonicated as previously described, electrophoresed on SDS-polyacrylamide gels, and transferred to Sequi-Blot PVDF membranes (Bio-Rad). Western blotting was performed with anti-γ H2AX (Ser-139), anti-p53, anti-phosphorylated p53 (Ser-15), anti-histone H3 and anti-phosphorylated histone H3 (Ser-10), and anti-β-actin at the indicated dilutions. Blots were incubated in a horseradish peroxidase-linked secondary antibody and the immune complex was detected using an enhanced chemiluminescence reaction kit (Millipore).

Flow cytometry. MIA PaCa-2 cells irradiated in the presence or absence of AZD2281 were trypsinized, fixed with 70% ethanol, treated with RNase A, stained with propidium iodide (PI) and analyzed by FACS Calibur (Beckton and Dickinson, Franklin Lakes, NJ, USA).

Statistical analysis. Statistical analysis was conducted using PASW Statistics 18 software (SPSS, Chicago, IL, USA). Levine's test was used to check the equality of variance. If the significance based on Levine's test was 0.05 or below, then probability was automatically calculated with Welch's *t*-test. Otherwise, the probability was calculated by Student's *t*-test. When the *P*-value was <0.05, the difference was considered statistically significant.

Results

Sensitization effect on γ-irradiation and carbon-ion irradiation. Figure 1 shows the dose-response curves of MIA PaCa-2 cells irradiated with γ-ray and carbon-ion beams with two different LET values (13 and 70 keV/μm) in the presence of the PARP inhibitor AZD2281. AZD2281-treated cells showed decreased survival both after γ-irradiation and carbon-ion irradiation compared to the controls. The enhancement ratios of AZD2281 at 1 and 5 μM are shown in Table 1. Isoeffective doses of γ-ray, LET13 carbon-ion and LET 70 carbon-ion irradiation that resulted in 10% cell survival were 5, 3.5 and 2.6 Gy, respectively. Therefore, cells were irradiated with 5 and 3 Gy doses of γ-ray and carbon-ion (LET 13 and 70) irradiation, respectively, for western blot analysis and flow cytometry.

Effect on double strand break levels. To analyze the effect of the PARP inhibitor on DSB, we used pulse field gel electrophoresis (PFGE) under neutral conditions. A 2-h exposure to AZD2281 induced an increase of DSB when the gel was analyzed after Southern blot hybridization. These induced DSB were diminished 12 h after incubation (Fig. 2A). Increase of DSB after 5 Gy of γ-irradiation was not detected in the absence or presence of AZD2281 between 5 and 24 h (data not shown).

Figure 2(B,C) shows the results of PFGE with ethidium bromide staining of DNA from cells at 18 h after carbon-ion irradiation. As described later, western blot analysis of cells irradiated with LET 13 and LET 70 carbon-ions showed a prolonged increase in the level of γ-H2AX, a DSB marker, when the cells were incubated for 10–24 h in the presence of PARP inhibitor. In the control cells, the repair occurred earlier, at 10 h. Therefore, we chose to analyze DSB in cells at 18 h by PFGE to demonstrate the increase in the level of persistent DSB caused by delayed repair in the presence of PARP inhibitor. LET 13 carbon-ion irradiation did not cause DSB with increasing radiation doses 18 h after irradiation in the presence of AZD2281 (Fig. 2B). By contrast, LET 70 carbon-ion irradiation increased the DSB level in a dose-dependent manner only in the presence of AZD2281 (Fig. 2C). A similar increase of DSB in the presence of PARP inhibitor was observed 24 h after LET 70 carbon-ion irradiation (data not shown).

Effect on DNA damage response. To further analyze the effect of PARP inhibition on DSB processing, the level of phosphorylated H2AX (γ-H2AX), which is a marker for DSB, was examined by western blot analysis. As shown in Figure 3(A,B) prolonged and increased levels of γ-H2AX were observed both after γ-irradiation and carbon-ion irradiation in the presence of the PARP inhibitor. The increase in the levels of γ-H2AX peaked 10 h after LET 13 irradiation alone. By contrast, the peak in γ-H2AX levels was shortened to 1-h post-irradiation in the presence of the PARP inhibitor. The persistent presence of γ-H2AX (arrow) and the 25-kDa form of γ-H2AX (marked with an asterisk), which is a mono-ubiquitinated form, was

doi: 10.1111/j.1349-7006.2012.02268.x

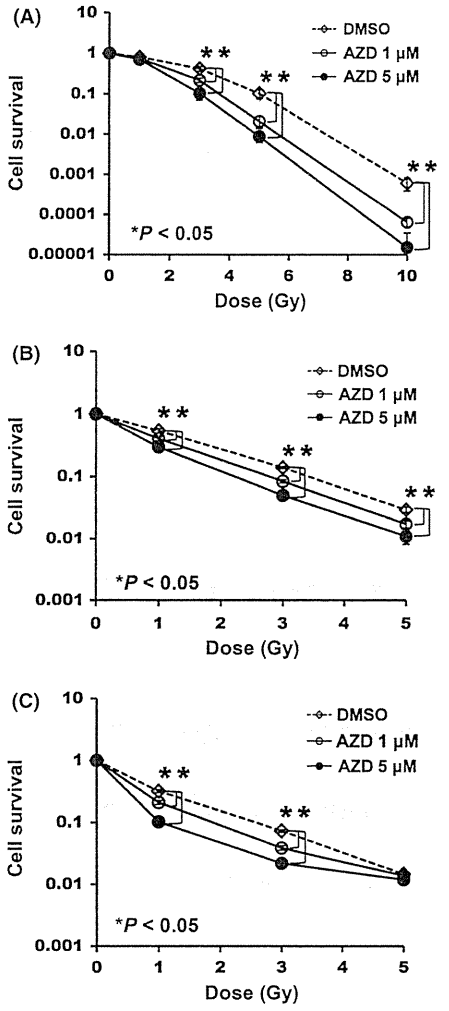

Fig. 1. (A) Clonogenic survival of MIA PaCa-2 cells treated with γ-irradiation alone and in combination with AZD2281. Surviving colonies (defined as > 50 cells) were counted after 5–6 days. The error bars indicate standard deviation calculated from three independent experiments. Asterisks and brackets indicate significant differences in response to γ-irradiation alone at $P < 0.05$. (A,B) Clonogenic survival of MIA PaCa-2 cells treated with liner energy transfer (LET) 13 keV/μm (B) and LET 70 keV/μm (C) carbon-ion irradiation alone and in combination with AZD2281. The cells were exposed to the indicated concentrations of AZD2281 for 2 h and irradiation was then performed. Experiments were carried out three times, and a representative result is shown. The error bars indicate standard deviation. Asterisks and brackets indicate significant differences in response to carbon-ion (LET 13 and 70 keV/μm) irradiation alone at $P < 0.05$.

Table 1. Enhancement ratios of radiosensitivity by AZD2281 at 10% survival

	γ-ray	Carbon-ion beam	
		LET 13 keV/μm	LET 70 keV/μm
AZD2281 1 μM	1.4	1.2	1.4
AZD2281 5 μM	1.7	1.5	2.5

LET, liner energy transfer.

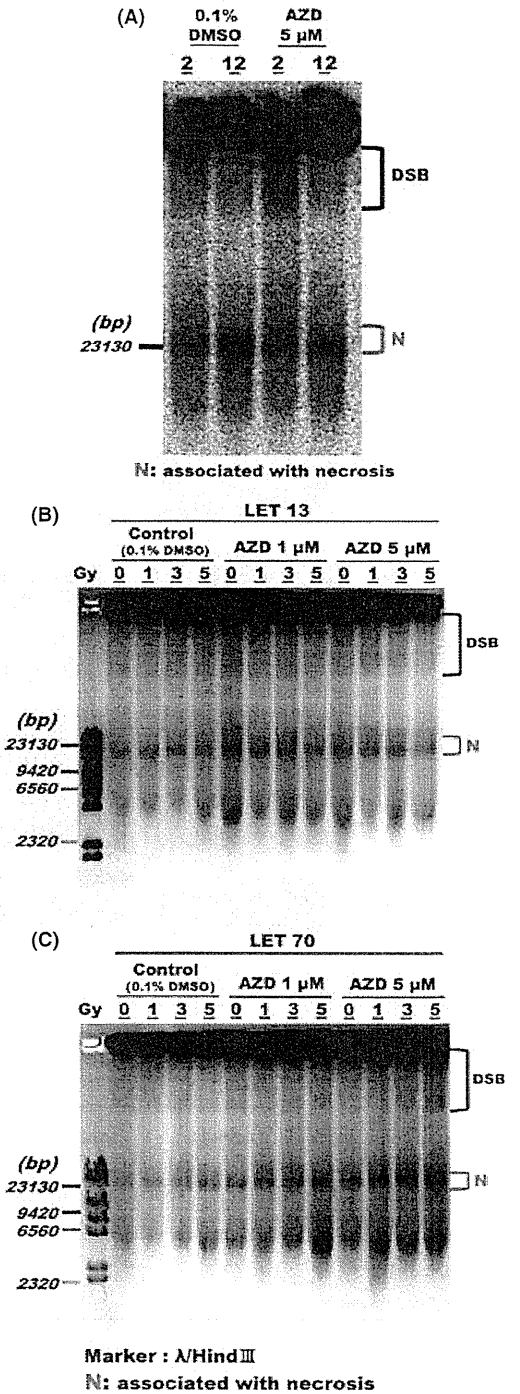

Fig. 2. The effect of double strand breaks (DSB) analyzed by neutral pulse field gel electrophoresis (PFGE). (A) The result of Southern blot analysis 2 and 12 h after addition of either AZD2281 or DMSO (control). (B,C) Ethidium bromide staining result of neutral PFGE 18 h after carbon-ion (liner energy transfer (LET) 13 keV/μm (B) and 70 keV/μm (C)) irradiation in the presence or absence of AZD2281. The positions of DSB and the bands associated with necrosis (N) are shown in brackets.

observed after LET 70 irradiation in the presence of AZD2281. Enhanced levels of p-p53 (Ser-15) were detected after γ-irradiation, but not after carbon-ion irradiation (Fig. 3B). In addition, decreased levels of phosphorylated histone H3, which is a G2/M marker, were observed after γ-irradiation and carbon-ion irradiation in the presence of AZD2281 compared

to its absence (Fig. 3A,B). Analysis of cell cycle progression using flow cytometry (Fig. 4) revealed that PARP inhibition induced S phase arrest and enhanced subsequent G2/M arrest both after γ-irradiation and LET 13 and 70 carbon-ion irradiation.

Discussion

In the present study, we have demonstrated that PARP inhibition is an effective radiosensitizer for carbon-ion irradiation. The underlying mechanism of radiosensitization by PARP inhibitors to both γ-irradiation and carbon-ion irradiation is suggested to be caused by a delay in DDR and DSB processing, which leads to increased S phase arrest and a subsequent arrest at the G2/M phase (Figs 3,4). Western blot analysis showed that this effect occurred independently of p53 phosphorylation status after carbon-ion irradiation. We speculate that these delays in DDR might be due to both the increase in persisting DSB generated by collapsed replication forks[10] and the effect of PARP inhibition on DSB repair pathways. Because MIA PaCa-2 cells did not show a subG1 apoptotic population either in the presence or absence of the PARP inhibitor (Fig. 4), but showed enhanced G2/M arrest, cell death through mitotic catastrophe or necrosis could be the plausible cell death pathways enhanced by the PARP inhibitor.[18]

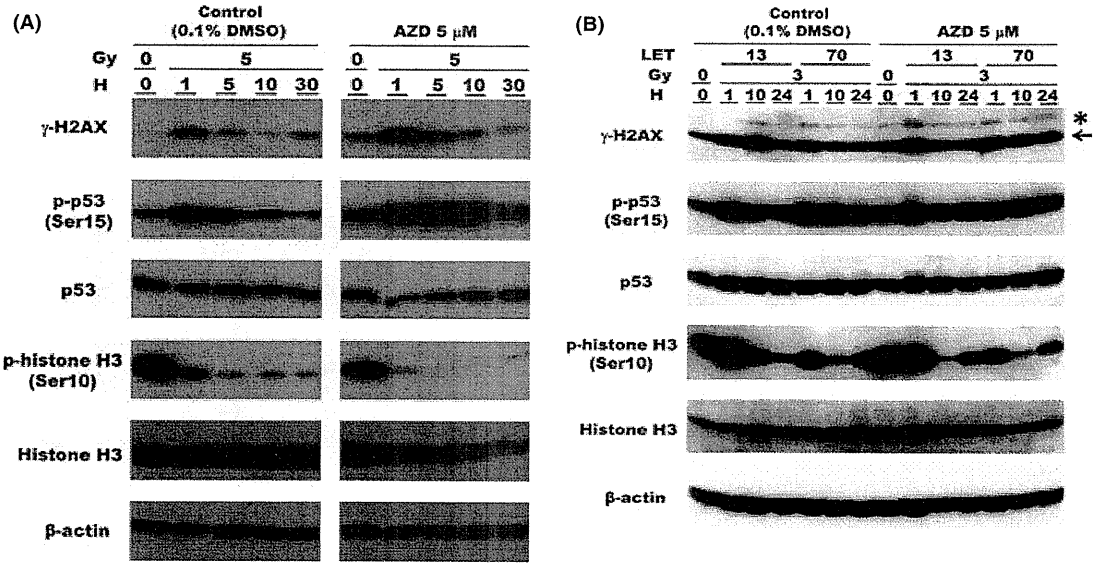

Fig. 3. The level of γ-H2AX, phosphorylated p53, p53, phosphorylated histone H3, histone H3 and β-actin, analyzed by western blotting after γ-irradiation at 5 Gy (A) or carbon-ion (liner energy transfer [LET] 13 and 70) irradiation at 3 Gy (B) in the presence or absence of AZD2281 at 5 μ. The arrow indicates γ-H2AX and an asterisk indicates mono-ubiquitinated γ-H2AX.

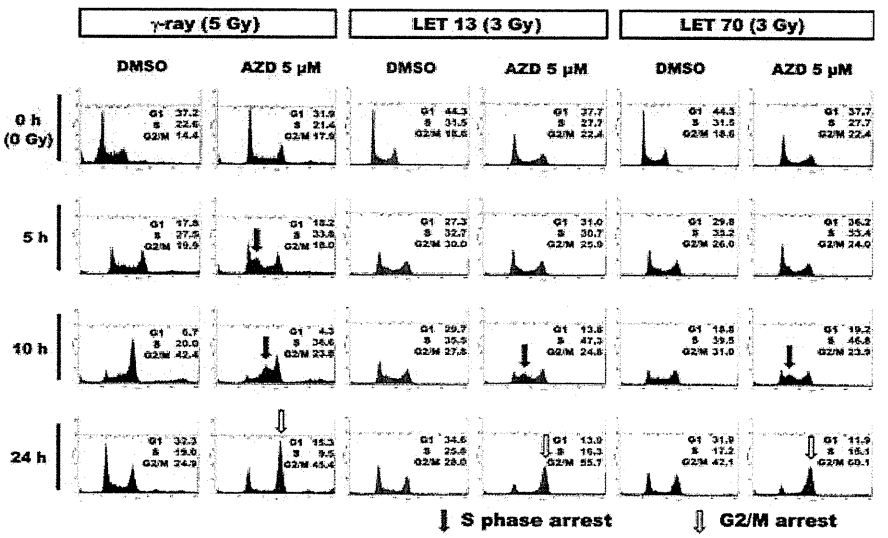

Fig. 4. Flow cytometry analysis with propidium iodide staining after γ-irradiation and carbon-ion irradiation. Percent distributions of cells in different phases of cell cycle are shown in each histogram. The black arrows indicate S phase arrest and the outlined arrows indicate G2/M arrest. The poly(ADP-ribose) polymerase (PARP) inhibitor AZD2281 induced S phase arrest and subsequent G2/M arrest both after γ-irradiation and carbon-ion irradiation.

doi: 10.1111/j.1349-7006.2012.02268.x

DNA damage induced by high LET heavy ion radiation is more complex than that caused by photons, and complex clustered DNA damage can be categorized into two major groups; namely, DSB and non-DSB oxidative clustered DNA lesions (OCDL).[19,20] OCDL are defined as two or more closely associated DNA lesions existing on both strands, usually within one or two helical turns.[19] Yields of clustered damage increase depending on the LET value.[21] OCDL include oxidized bases, apurinic–apyrimidinic sites and SSB, and these lesions are repaired mainly by BER, in which PARP plays a significant role.

We speculate that the sensitization effect of PARP inhibitors on carbon-ion irradiation may be mediated by the conversion of sub-lethal OCDL to lethal damage caused by blocking the BER pathway. Consistent with these premises, the survival curve parameters and the effects of the PARP inhibitor were quite different dependent on what type of irradiation was used; γ-ray resulted in a distinct shoulder on the survival curve, which was not present with LET 13, and was small with LET 70 at the higher dose range close to log-linear. This difference in the survival curve parameters could result in differences in the enhancement ratios, as shown in Table 1. In the presence of 5 μM PARP inhibitor, the enhancement ratio at 10% survival was higher for LET 70 carbon-ion irradiation than for γ-ray and LET 13 (ER_{10}:1.7 for γ-ray, 1.5 for LET 13 and 2.5 for LET 70).

At the lower doses that gave more than 10% survival, PARP inhibitor could affect cell death on OCDL induced by LET 70 carbon-ion irradiation. At the higher dose that gave lower than 10% survival, namely, at 5 Gy of LET 70 carbon-ion irradiation, the amount of clustered lethal DSB may increase and be a main cause of cell death. Thus, the effects of AZD on OCDL or SSB may not contribute much to cell death. This could be the reason why we could not detect the sensitization effect of the PARP inhibitor in the present study at 5 Gy of LET 70 carbon-ion irradiation. In contrast, for γ-irradiation and LET 13 carbon-ion irradiation, the ratio of clustered lethal DSB is low and the amount of SSB and OCDL, which are repaired by the BER pathway, increases dose-dependently so that AZD2281 could sensitize more at higher doses of irradiation. Therefore, the PARP inhibitor enhanced the effect of LET 70 carbon-ion irradiation at a lower dose than 5 Gy and enhanced the effects of γ-irradiation and LET 13 carbon-ion irradiation at all doses.

Conversion of OCDL to lethal DSB by binding of the PARP inhibitor to PARP at strand break ends may be more effective with OCDL produced by LET 70 carbon-ion irradiation compared to those produced by γ-irradiation and LET 13 carbon-ion irradiation. This could be the reason why we observed a higher enhancement ratio by the PARP inhibitor for LET 70 carbon-ion irradiation at low doses.

Therefore, the effect of PARP inhibition on clustered damage should be analyzed further. However, our results suggest that inhibition of PARP sensitizes cells to various forms of radiation by affecting the repair of OCDL, which leads to a delay of the DDR. The effect of PARP inhibition on DSB repair pathways is also thought to be an important mechanism for sensitization to carbon-ion irradiation. These results imply that the PARP inhibitor might sensitize cells at low doses (i.e. 3 Gy or less) of carbon-ion irradiation at the Bragg peak more than at the entrance region. Therefore, doses lower than 5 Gy of LET 70 carbon-ion irradiation could be the appropriate range of radiosensitization with a blockade of DNA repair by PARP inhibitor.

As the sensitization effect of PARP inhibitors combined with photon beams is well characterized *in vitro* and *in vivo*, it is important to compare the sensitizing effect of PARP inhibitors for proton and other types of radiation with clinical applications. Furthermore, radiosensitizers for charged particle radiation therapy evaluated using animal models should show a lower cell-killing effect on normal cells at the entrance region and a pronounced definite effect on cancer cells at spread-out Bragg peaks.[22]

Few factors are known to induce sensitization to charged particle radiation, and we have demonstrated that PARP inhibition is a radiosensitizer for carbon-ion irradiation. The present results show that the inhibition of PARP enhances radiosensitivity to γ-ray and carbon-ion irradiation by disturbing DDR, possibly by increasing the conversion of non-DSB lesions to lethal DNA damage, and suggest that functional inhibition of PARP should be useful for sensitizing to both low and high LET radiation therapies.

Acknowledgments

This research was conducted as a Research Project at NIRS-HIMAC (21B366). We appreciate the help and suggestions provided by the HIMAC support team, and Dr Akira Fujimori at the NIRS, and Dr Shunpei Onami, Dr Hitoshi Nakagama and Dr Takashi Sugimura at the National Cancer Center. This work was supported in part by a Grant-in-Aid for Cancer Research from the Ministry of Health, Labor and Welfare of Japan (19-9), by the National Cancer Center Research and Development Fund (H23-A-43), by a Grant-in-Aid for Scientific Research from the Ministry of Education, Science, Sports, and Culture of Japan (22300343), and by the Third Term Comprehensive 10-Year Strategy for Cancer Control. H. T. is an awardee of the Resident Fellowship from the Foundation for Promotion of Cancer Research (Japan) for the 3rd Term Comprehensive 10-Year Strategy for Cancer Control.

Disclosure Statement

The authors have no conflict of interest.

References

1 Tsujii H Mizoe JE Kamada T *et al.* Overview of clinical experiences on carbon ion radiotherapy at NIRS. *Radiother Oncol* 2004; **73**(Suppl 2): S41–9.
2 Blakely EA Kronenberg A. Heavy-ion radiobiology: new approaches to delineate mechanisms underlying enhanced biological effectiveness. *Radiat Res* 1998; **150**: S126–45.
3 Tofilon PJ Camphausen K. Molecular targets for tumor radiosensitization. *Chem Rev* 2009; **109**: 2974–88.
4 Schreiber V Dantzer F Ame JC *et al.* Poly(ADP-ribose): novel functions for an old molecule. *Nat Rev Mol Cell Biol* 2006; **7**: 517–28.
5 O'Shaughnessy J. Triple negative breast cancer: the emerging treatment with BSI-201 (Iniparib). *Oncologist* 2010; **15**: 1–7.
6 Farmer H McCabe N Lord CJ *et al.* Targeting the DNA repair defect in BRCA mutant cells as a therapeutic strategy. *Nature* 2005; **434**: 917–21.
7 Fong PC Boss DS Yap TA *et al.* Inhibition of poly(ADP-ribose) polymerase in tumors from BRCA mutation carriers. *N Engl J Med* 2009; **361**: 123–34.
8 Fong PC Yap TA Boss DS *et al.* Poly(ADP)-ribose polymerase inhibition: frequent durable responses in BRCA carrier ovarian cancer correlating with platinum-free interval. *J Clin Oncol* 2010; **28**: 2512–19.
9 O'Shaughnessy J Osborne C Pippen JE *et al.* Iniparib plus chemotherapy in metastatic triple-negative breast cancer. *N Engl J Med* 2011; **364**: 205–14.
10 Dungey FA Loser DA Chalmers AJ. Replication-dependent radiosensitization of human glioma cells by inhibition of poly(ADP-Ribose) polymerase: mechanisms and therapeutic potential. *Int J Radiat Oncol Biol Phys* 2008; **72**: 1188–97.
11 Efimova EV Mauceri HJ Golden DW *et al.* Poly(ADP-ribose) polymerase inhibitor induces accelerated senescence in irradiated breast cancer cells and tumors. *Cancer Res* 2010; **70**: 6277–82.

12 Senra JM Telfer BA Cherry KE *et al.* Inhibition of PARP-1 by Olaparib (AZD2281) Increases the radiosensitivity of a lung tumor xenograft. *Mol Cancer Ther* 2011; **10**: 1949–58.
13 Fisher AE Hochegger H Takeda S *et al.* Poly(ADP-ribose) polymerase 1 accelerates single-strand break repair in concert with poly(ADP-ribose) glycohydrolase. *Mol Cell Biol* 2007; **27**: 5597–605.
14 Chalmers AJ. The potential role and application of PARP inhibitors in cancer treatment. *Br Med Bull* 2009; **89**: 23–40.
15 Suzuki M Kase Y Yamaguchi H *et al.* Relative biological effectiveness for cell-killing effect on various human cell lines irradiated with heavy-ion medical accelerator in Chiba (HIMAC) carbon-ion beams. *Int J Radiat Oncol Biol Phys* 2000; **48**: 241–50.
16 Hamada N Imaoka T Masunaga S *et al.* Recent advances in the biology of heavy-ion cancer therapy. *J Radiat Res (Tokyo)* 2010; **51**: 365–83.
17 Shibata A Kamada N Masumura K *et al.* Parp-1 deficiency causes an increase of deletion mutations and insertions/rearrangements in vivo after treatment with an alkylating agent. *Oncogene* 2005; **24**: 1328–37.
18 Roninson IB Broude EV Chang BD. If not apoptosis, then what? Treatment-induced senescence and mitotic catastrophe in tumor cells. *Drug Resist Updat* 2001; **4**: 303–13.
19 Hada M Georgakilas AG. Formation of clustered DNA damage after high-LET irradiation: a review. *J Radiat Res (Tokyo)* 2008; **49**: 203–10.
20 Okayasu R. Repair of DNA damage induced by accelerated heavy ions-a mini review. *Int J Cancer* 2012; **130**: 991–1000.
21 Hada M Sutherland BM. Spectrum of complex DNA damages depends on the incident radiation. *Radiat Res* 2006; **165**: 223–30.
22 Kanai T Furusawa Y Fukutsu K *et al.* Irradiation of mixed beam and design of spread-out Bragg peak for heavy-ion radiotherapy. *Radiat Res* 1997; **147**: 78–85.

doi: 10.1111/j.1349-7006.2012.02268.x

SCIENTIFIC REPORTS

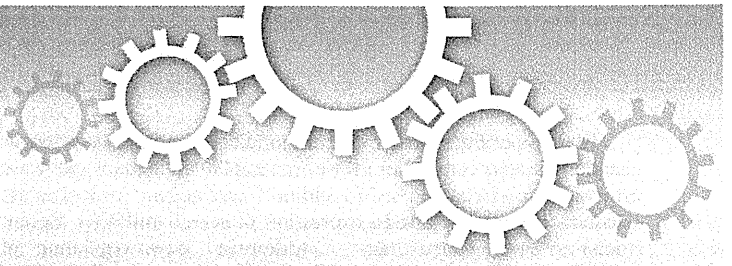

OPEN

SUBJECT AREAS:
NON-CONDING RNA'S
RNAI
SMALL RNA'S
TUMOUR SUPPRESSORS

Received
1 December 2011

Accepted
24 February 2012

Published
15 March 2012

Correspondence and requests for materials should be addressed to T.O. (tochiya@ncc.go.jp)

Stilbene derivatives promote Ago2-dependent tumour-suppressive microRNA activity

Keitaro Hagiwara[1,2], Nobuyoshi Kosaka[1], Yusuke Yoshioka[1], Ryou-u Takahashi[1], Fumitaka Takeshita[1] & Takahiro Ochiya[1,2]

[1]Division of Molecular and Cellular Medicine, National Cancer Center Research Institute, 5-1-1, Tsukiji, Chuo-ku, Tokyo 104-0045, Japan, [2]Department of Biological Sciences, Tokyo Institute of Technology, 4259 Nagatsuta-cho, Midori-ku, Yokohama 226-8501, Japan.

It is well known that natural products are a rich source of compounds for applications in medicine, pharmacy, and biology. However, the exact molecular mechanisms of natural agents in human health have not been clearly defined. Here, we demonstrate for the first time that the polyphenolic phytoalexin resveratrol promotes expression and activity of Argonaute2 (Ago2), a central RNA interference (RNAi) component, which thereby inhibits breast cancer stem-like cell characteristics by increasing the expression of a number of tumour-suppressive miRNAs, including miR-16, -141, -143, and -200c. Most importantly, resveratrol-induced Ago2 resulted in a long-term gene silencing response. We also found that pterostilbene, which is a natural dimethylated resveratrol analogue, is capable of mediating Ago2-dependent anti-cancer activity in a manner mechanistically similar to that of resveratrol. These findings suggest that the dietary intake of natural products contributes to the prevention and treatment of diseases by regulating the RNAi pathway.

Natural products are a rich source of valuable medicinal agents. More than half of the currently available drugs are natural or related compounds. In the case of cancer, the percentage of natural compounds exceeds 60%. Research on natural products as potential anti-cancer agents dates back to at least the Egyptian Ebers Papyrus of 1550 B.C. However, more recent scientific investigations began with the studies of Hartwell and co-workers on the application of podophyllotoxin and its derivatives as anti-cancer agents[1]. A large number of plant, marine, and microbial sources have been tested, and hundreds of active compounds have been isolated. Despite these advances, the underlying mechanisms of natural products in human health are not fully understood.

Resveratrol, which is a multi-functional polyphenolic compound, is a phytoalexin present in a wide variety of plant species, including grapes, mulberries, and peanuts[2]. Since its discovery, resveratrol has been shown to exhibit a plethora of physiological properties that may be useful in human medicine. More interest was focused on resveratrol at the beginning of the 1990s when it was first shown to be present in red wine[3]. Experimental studies have shown that resveratrol inhibits the growth of various cancer cells and induces apoptotic cell death[4,5]. Recently, a phase I/II clinical trial in patients with colon cancer was conducted to examine the effects of resveratrol treatment on colon cancer progression and colonic mucosa in patients with colon cancer and its effects in modulating the Wnt signalling pathway[2]. Although these data provide evidence of multiple anti-tumour effects induced by resveratrol, the exact mechanism is not clearly understood.

MicroRNAs (miRNAs) have emerged as key post-transcriptional regulators of gene expression that are involved in diverse physiological and pathological processes[6]. The inhibition of the miRNA biogenesis pathway results in severe developmental defects and lethality in many organisms[7]. It has been suggested that a considerable number of miRNAs have roles in cancer cells. Indeed, an increasing number of experimental studies have shown that the knock-down or the re-expression of specific miRNAs could induce drug sensitivity, inhibit the proliferation of cancer cells, and suppress cancer cell invasion and metastasis[8–10]. Recent studies have shown that natural products, including curcumin, isoflavone, I3C, DIM, and EGCG, could alter the expression of specific miRNAs, which may lead to the increased sensitivity of cancer cells to conventional anti-cancer agents and, therefore, tumour growth inhibition[11–14]. However, the exact molecular mechanism of miRNA induction and the biological significance of resveratrol-induced miRNAs have not been reported.

Diet is one of the most important modifiable cancer risk determinants[15]. Dietary components have been implicated in many pathways involved in carcinogenesis. In addition, carcinogenic processes are associated with the altered expression of several miRNAs. Recent studies have reported that a widespread down-regulation of miRNAs is commonly observed during human cancer-cell initiation and progression[16,17]. In this study, we hypothesised that the dietary intake of natural products maintains tumour-suppressive miRNA expression in cancer cells, leading to the prevention of carcinogenesis. We demonstrated that resveratrol suppresses cancer cell malignancy *in vitro* and *in vivo* through the transcriptional activation of tumour-suppressive miRNAs and Argonaute2 (Ago2). Furthermore, we provided evidence that Ago2 over-expression enhances the RNA interference (RNAi) activity. These findings suggest that the dietary intake of natural products safely reduces a wide range of negative consequences with an overall improvement in human health and survival by modulating miRNA biogenesis.

Results

Resveratrol reduces the cancer stem-like cells population by up-regulating miR-141 and miR-200c. To identify the potential anti-cancer activity of resveratrol, we investigated the effects of this compound on tumour formation *in vivo*. We orthotopically inoculated female SCID hairless outbred mice with MDA-MB-231-luc-D3H2LN cells (200 cells), which were then treated with resveratrol (25 mg/kg/day) or ethanol (control) via intraperitoneal injection every day for one week. Tumour growth was then monitored using an IVIS imaging system. The weight of the mice did not significantly change between the groups during the course of the experiment, suggesting that resveratrol did not have notable adverse effects on mice (Supplementary Fig. 1a). The results demonstrated that the resveratrol administration into the mice significantly suppressed tumour formation, while obvious tumours were observed in vehicle-treated mice, indicating that resveratrol is capable of inhibiting the survival and growth of cancer cells *in vivo* (Fig. 1a). A recent report has shown that solid tumours contain a distinct population of cells with the ability to form tumours in mice; these cells are known as tumour-initiating or cancer stem-like cells (CSCs) and display increased drug resistance and metastatic ability because they consistently form tumours, whereas other cancer cell populations were depleted of cells capable of tumour formation[18,19]. To identify the effects of resveratrol on the CSC phenotype, breast cancer cells were examined for changes in the CSC population, which is a highly tumourigenic $CD44^+/CD24^-$ subpopulation with stem cell-like self-renewal properties and the ability to produce differentiated progeny after resveratrol treatment[18]. Compared to vehicle-treated control cells, cells treated with 50 μM resveratrol demonstrated a significant 6-fold decrease in the $CD44^+/CD24^-$ population in MDA-MB-231-luc-D3H2LN cells (Fig. 1b). In addition, mammosphere formation, which has been widely used for breast CSC enrichment, of the $CD44^+/CD24^-$ fraction from MDA-MB-231-luc-D3H2LN cells was suppressed after resveratrol treatment (Supplementary Fig. 1b). We also assessed apoptosis using TUNEL staining and a caspase assay and found that resveratrol did not induce apoptosis (Supplementary Figs. 1c and 1d). Human breast cancers are driven by a CSC component that may contribute to tumour metastasis and therapeutic resistance[20]. Indeed, we found that the combination of resveratrol with low therapeutic doses of docetaxel elicits significantly greater cancer cell growth inhibition *in vitro* and *in vivo* (Supplementary Figs. 1e–g). These findings strongly suggest that resveratrol demonstrates multiple anti-cancer effects through the reduction of the CSC population.

To examine whether resveratrol could influence the breast cancer cell metastasis ability, the highly invasive breast cancer cell line MDA-MB-231-luc-D3H2LN was used in *in vitro* invasion assays. As shown in Fig. 1c, the invasion of MDA-MB-231-luc-D3H2LN cells was suppressed by resveratrol treatment. Previous studies have documented aberrant miRNA expression in cancer, and our observations prompted us to hypothesise that the anti-cancer resveratrol effects were mediated by miRNAs, particularly by a group of tumour-suppressive miRNAs[21]. A recent study has demonstrated that miR-141 and miR-200c strongly inhibit breast cancer invasion ability[22]. We found that resveratrol exposure increases miR-141 and miR-200c expression in MDA-MB-231-luc-D3H2LN cells (Fig. 1d). These findings suggest that resveratrol exhibits multiple anti-cancer effects through the inhibition of CSC phenotypes by activating miR-141 and miR-200c. In addition, to determine whether the up-regulation of miR-141 and miR-200c is mediated at the transcriptional level, we measured the expression levels of the primary miRNAs of miR-141 and miR-200c and found that these miRNAs are up-regulated at the primary transcript level (Supplementary Fig. 1h). Taken together, these results indicate that resveratrol increases the expression of tumour-suppressive miRNAs via the induction of miRNA transcription. Similar results were obtained in two other human breast cancer cell lines (MCF7 and MCF7-ADR) and MCF10A, an immortalised, non-transformed epithelial cell line (Supplementary Figs. 2–4).

Resveratrol up-regulates the expression of tumour-suppressive miRNAs. We demonstrated that resveratrol specifically reduced the CSC fraction (Fig. 1b). In addition, we also observed that miR-141 and miR-200c, which are known to suppress the CSC phenotype, are both induced by resveratrol treatment (Fig. 1d). These observations suggest that a part of the anti-cancer effects of resveratrol is mediated by miRNAs, particularly tumour-suppressive miRNAs. Indeed, a morphological change is observed after resveratrol treatment (Fig. 2a), suggesting that resveratrol induces a variety of miRNAs in cancer cells. To confirm whether miRNAs are globally up-regulated in the multiple anti-cancer effects induced by resveratrol in MDA-MB-231-luc-D3H2LN cells, we performed a comprehensive miRNA profiling of untreated MDA-MB-231-luc-D3H2LN cells and compared the results to those obtained in resveratrol-treated cells. As shown in Fig. 2b, we found that a subset of tumour-suppressive miRNAs is transcriptionally up-regulated by resveratrol (Table 1). To validate the microarray results, we performed qRT-PCR. A set of mature tumour-suppressive miRNAs, including miR-16 and miR-143, are significantly up-regulated in a variety of breast cancer cell lines, including MDA-MB-231-luc-D3H2LN, MCF7, MCF7-ADR, and MCF10A (Supplementary Figs. 2–5). These results indicated that resveratrol globally up-regulates tumour-suppressive miRNAs in human breast normal epithelial and cancer cells.

Resveratrol enhances the Ago2 RNAi potency. Although our data provide evidence that resveratrol globally up-regulates tumour-suppressive miRNAs and one of the mechanisms that is mediated by primary miRNA up-regulation, we also hypothesised that changes at other levels of the RNAi pathway may play a role in enhancing the resveratrol-mediated miRNA activity in cells in addition to transcriptional alterations. It is known that miRNA generation occurs in a multi-step process[23,24]. If one of the components associated with the miRNA pathway is under-expressed or qualitatively impaired, the pathway as a whole is destabilised. To examine the effect of resveratrol on the miRNA machinery, we measured the expression levels of a selected group of miRNA machinery-related genes, including Dicer1, Drosha, TARBP2, DGCR8, and Ago2, after the resveratrol treatment of MDA-MB-231-luc-D3H2LN cells. We found that resveratrol exposure significantly increased Ago2 expression in MDA-MB-231-luc-D3H2LN cells (Fig. 2c and Supplementary Fig. 6a). To elucidate the resveratrol-mediated Ago2 up-regulation mechanism, we assessed the Ago2 promoter activity and the Ago2 mRNA and protein half-lives after resveratrol treatment. As shown in supplementary Fig. 6b, the Ago2 protein half-lives were unchanged after resveratrol treatment. In contrast, the Ago2 mRNA was slightly

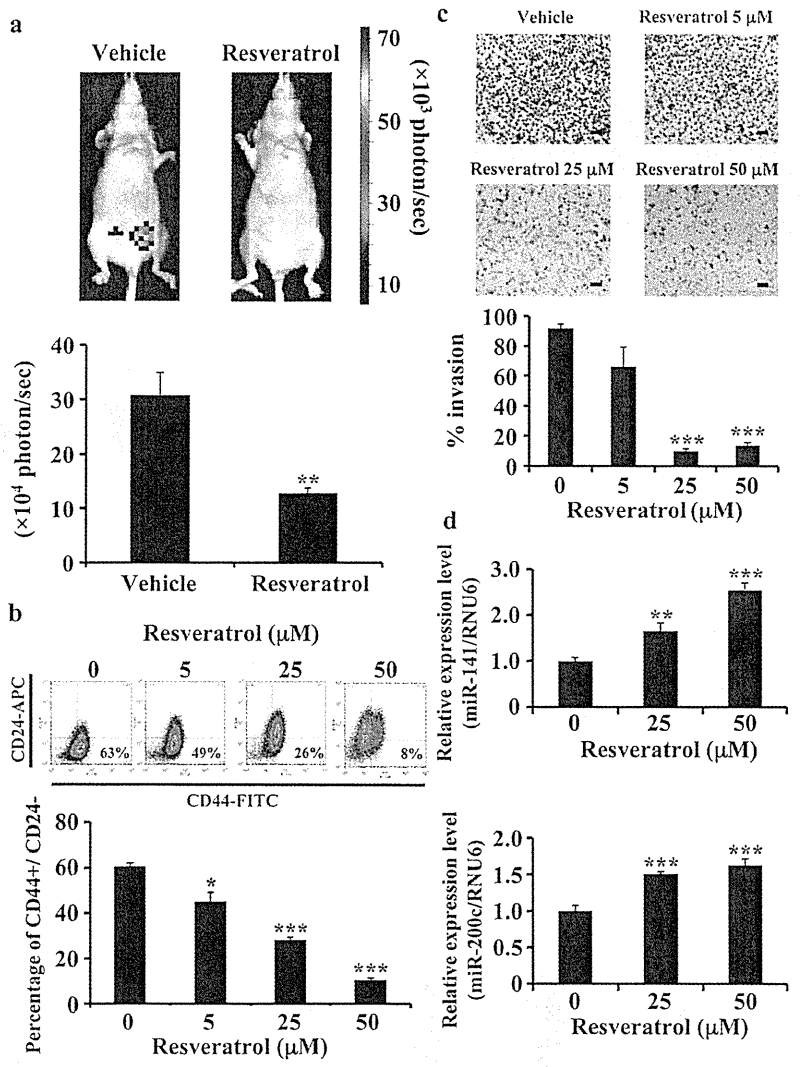

Figure 1 | Multiple anti-cancer effects of resveratrol through the activation of miR-141 and miR-200c. (a) MDA-MB231-luc-D3H2LN cells (200 cells) were injected into the mammary fat pad of six-week-old female SCID hairless outbred mice (n = 5). They were then treated with resveratrol (25 mg/kg/day) by intraperitoneal injection every day for 8 days. Tumour growth was monitored by injecting luciferin in the mice followed by measuring bioluminescence using an IVIS imaging system. Representative mouse images at day 8 (upper panel) and quantified bioluminescence images at day 8 (lower panel) are shown. (b) MDA-MB231-luc-D3H2LN cells were treated with resveratrol or DMSO (control) at the specified doses for 3 days. The percentage of $CD44^+/CD24^-$ cells after compound treatment in independent experiments with MDA-MB231-luc-D3H2LN cell populations is shown. The $CD44^+/CD24^-$ denoting the CSC-enriched fraction. (c) MDA-MB231-luc-D3H2LN cells were grown, treated with resveratrol or DMSO (control) for 1 day, and then subjected to an invasion assay. Representative photographs (upper panel) and quantification (lower panel) are shown. Scale bar: 100 μm. (d) The miR-141 and miR-200c expression levels in MDA-MB231-luc-D3H2LN cells. The expression levels of the indicated miRNAs were examined in MDA-MB231-luc-D3H2LN cells after 48 hour resveratrol treatment (all data are shown as the mean ± s.e.m., *P<0.05, **P<0.01, ***P<0.001).

increased after resveratrol treatment (Supplementary Fig. 6c). In addition, resveratrol induced the luciferase activity of a plasmid containing the Ago2 promoter upstream of the luciferase gene, suggesting that resveratrol transcriptionally induced the expression of Ago2 (Supplementary Fig. 6d). The Ago2 protein is a key regulator of miRNA homeostasis and, upon recognition, it can either cleave or remain tethered to an mRNA to repress its translation and/or regulate its stability[25]. To reveal the relationship between Ago2 and miRNAs, we first quantified the miRNA expression in MDA-MB-231-luc-D3H2LN cells transfected with the Ago2 expression vector. The induction of Ago2 expression by the Ago2 expression vector was confirmed by qRT-PCR (Fig. 2d). After transfection of the Ago2 expression vector, a subset of miRNAs including miR-16, miR-141, miR-143, and miR-200c was higher than in the control cells (Fig. 2e and Supplementary Fig. 6e). To further study the relationship between resveratrol-induced Ago2 and RNAi activity, MDA-MB-231-luc-D3H2LN cells were transfected with luciferase siRNA in the presence of resveratrol treatment and subjected to an *in vitro* firefly luciferase assay. If the induction of Ago2 expression leads to the enhancement of RNAi activity in cells, the luciferase siRNA silencing effect of the luciferase gene in MDA-MB-231-luc-D3H2LN cells may be enhanced after Ago2 over-expression even in the presence of a low siRNA dose and a prolonged period after siRNA transfection. As shown in Fig. 2f, the resveratrol-induced Ago2 resulted in a long-term gene-silencing response in MDA-MB-231-luc-D3H2LN cells. In addition, Ago2 over-expression in HEK293 cells demonstrated a long-term gene-silencing response that was similar to resveratrol-treated MDA-MB-231-luc-D3H2LN cells (Supplementary Fig. 6f).

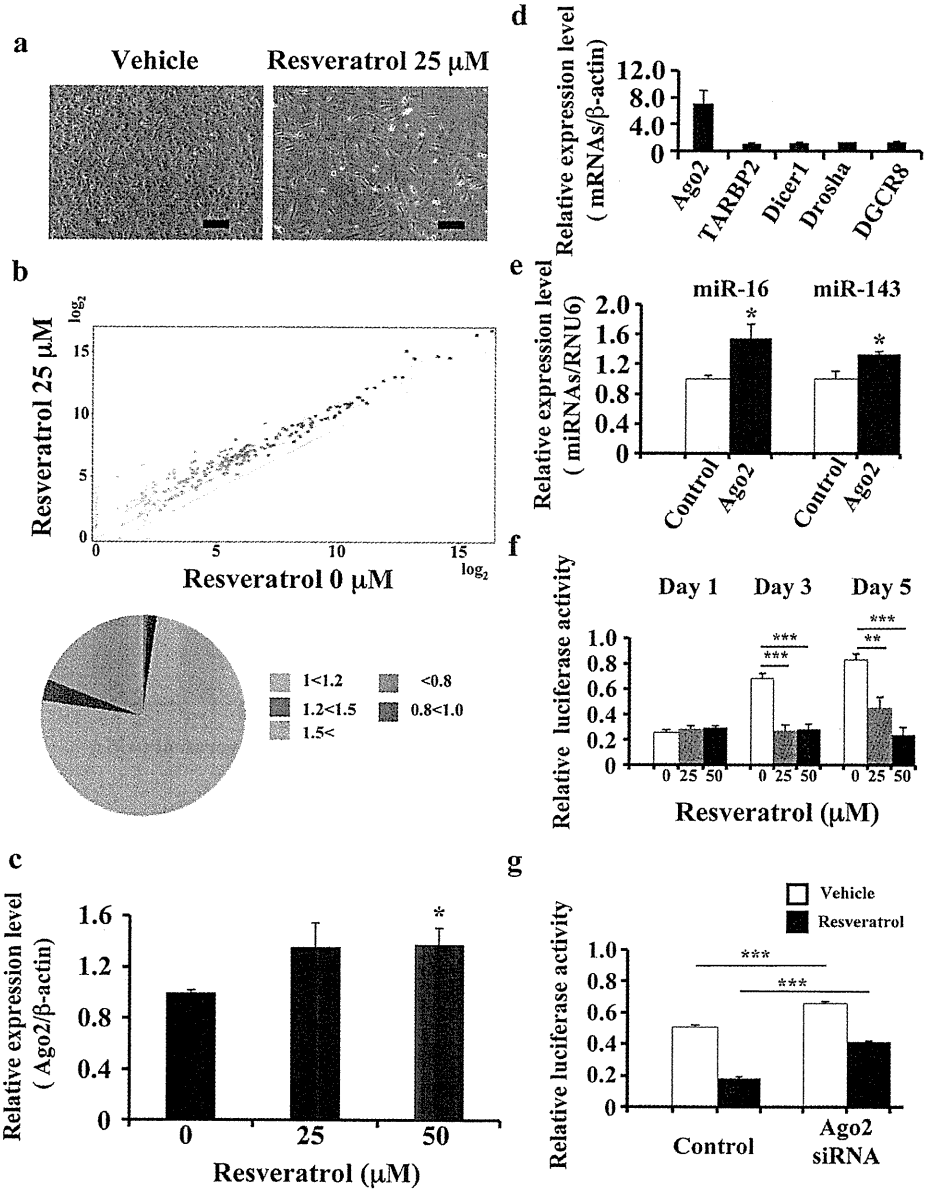

Figure 2 | Association between resveratrol and Ago2. (a) Characteristic microscopic images of MDA-MB231-luc-D3H2LN cells in the presence of DMSO (control) or resveratrol. Scale bar: 100 μm. (b) The effects of resveratrol treatment on miRNA expression in MDA-MB231-luc-D3H2LN cells by miRNA microarray analysis. The proportions of miRNAs at different fold change levels are shown in the lower panel. (c) MDA-MB231-luc-D3H2LN cells were treated with resveratrol or DMSO (control). After 2 days of culture, the cell extract was subjected to real-time mRNA qRT-PCR. (d), (e) MDA-MB231-luc-D3H2LN cells were grown and transiently transfected with Ago2 or EGFP-IRES vector (control). After 2 days of culture, the cell extract was subjected to real-time mRNA (d) and miRNA (e) qRT-PCR. The values on the *y-axis* are depicted relative to the expression level of the EGFP-IRES control vector, which is defined as 1. (f) MDA-MB231-luc-D3H2LN cells were grown and transiently transfected with luciferase siRNA or AllStars negative control siRNA (0.1 nM) under resveratrol treatment. After 1, 3, or 5 days of culture, the cells were subjected to a luciferase reporter assay. The values on the *y-axis* are depicted relative to the luciferase activity of the AllStars Negative Control siRNA, which is defined as 1. (g) MDA-MB231-luc-D3H2LN cells were grown and transiently transfected with luciferase siRNA or AllStars Negative Control siRNA and Ago2 siRNA or AllStars Negative Control siRNA. After 3 days of culture, the cells were subjected to a luciferase reporter assay. The values on the *y-axis* are depicted relative to the luciferase activity of the negative control siRNA, which is defined as 1 (all data are shown as the mean ± s.e.m., *P<0.05, **P<0.01, ***P<0.001).

Moreover, we performed an RNAi experiment to target Ago2 after resveratrol treatment and then assessed the RNAi activity demonstrated by the luciferase siRNA directed against the luciferase gene. The reduction in Ago2 expression by Ago2 siRNA was confirmed by qRT-PCR (Supplementary Fig. 6g). As shown in Fig. 2g, Ago2 siRNA-mediated silencing inhibited the RNAi activity in MDA-MB-231-luc-D3H2LN cells. Taken together, these results indicate that the resveratrol anti-cancer activities were mediated by not only tumour suppressive miRNA upregulation but also by the enhancement of the RNAi activity regulated by Ago2.

Resveratrol-induced miRNA exert an anti-cancer effect. It has been reported that miR-141 inhibits the epithelial-mesenchymal transition and cancer cell migration in breast cancer cells[26]. In addition, we found that resveratrol induced the expression of miR-141 and miR-200c in MDA-MB-231-luc-D3H2LN cells (Fig. 1d). In

Table 1 | A list of miRNAs which were up-regulated more than 2.0-fold by resveratrol in MDA-MB-231-luc-D3H2LN cells compared with control

miRNA	Fold change
Tumor-suppressive miRNA	
hsa-miR-141	4.48
hsa-miR-26a	2.33
hsa-miR-195	3.38
hsa-miR-126	2.41
hsa-miR-185	2.75
hsa-miR-340	11.07
hsa-miR-128	2.13
hsa-miR-34a	2.65
hsa-miR-193b	2.58
hsa-miR-335	2.42
hsa-miR-200c	3.47
hsa-miR-196a	2.67
hsa-miR-497	4.60
hsa-miR-125a-3p	3.00
Onco- miRNA	
hsa-miR-378*	4.81
hsa-miR-10b	5.11
hsa-miR-132	7.23
hsa-miR-222	2.40

contrast, the CSC population was decreased (Fig. 1b). To show direct evidence of whether multiple phenotypes induced by resveratrol were regulated by tumour-suppressive miRNAs, MDA-MB-231-luc-D3H2LN cells were transfected with an antisense oligonucleotide targeting miR-141 (i.e., a miR-141 inhibitor) in the presence of resveratrol treatment. MiR-141 repression by the miR-141 inhibitor was confirmed by qRT-PCR (supplementary Fig. 7a). As shown in Fig. 3a, the miR-141-induced inhibition of invasion was abrogated by the addition of the miR-141 inhibitor, and the MDA-MB-231-luc-D3H2LN cell invasiveness was increased. To confirm the link between resveratrol and miRNA expression, we investigated the growth of breast cancer cells in the presence or absence of a miR-143 inhibitor[27]. In the presence of resveratrol, miR-143-induced inhibition significantly increased the survival of MDA-MB-231-luc-D3H2LN cells relative to the control (Fig. 3b). It has been shown that miR-200c up-regulation in breast cancer cells inhibits Zeb1 expression, resulting in E-cadherin induction in breast cancer cell lines[28]. As shown in Fig. 1d, we found miR-200c up-regulation after resveratrol treatment, suggesting that resveratrol treatment activates this pathway and demonstrating its anti-cancer activity. Indeed, resveratrol addition significantly suppressed Zeb1 expression in the breast cancer cell lines (Fig. 3c) and induced E-cadherin expression in those cells (supplementary Fig. 7b). Furthermore, to show the direct effects of resveratrol on the miRNA machinery, we performed a Zeb1 3′UTR assay and demonstrated that resveratrol treatment significantly down-regulated the luciferase activity of a plasmid containing the Zeb1 3′UTR (Fig. 3d). Taken together, these results suggested that resveratrol plays an important role in breast cancer prevention by up-regulating tumour-suppressive miRNAs.

The stilbene family regulates miRNA biogenesis. The naturally occurring dimethylether resveratrol analogue pterostilbene is a stilbene family member that is generated by plants. Pterostilbene has also been reported to possess chemopreventive activity in cancer and other resveratrol-like health benefits[29,30]. To determine whether pterostilbene induced the expression of tumour-suppressive miRNAs in a similar manner as resveratrol, we assessed the effect of pterostilbene on miRNA expression. As shown in Fig. 4a, pterostilbene treatment suppressed cell growth more significantly than resveratrol treatment in MDA-MB-231-luc-D3H2LN cells. In addition, the expression of tumour suppressive miRNAs (i.e., miR-143 and miR-200c) and Ago2 was significantly higher in pterostilbene-treated MDA-MB-231-luc-D3H2LN cells than in resveratrol-treated cells (Figs. 4b-d and Supplementary Fig. 8). Taken together, these results suggest that resveratrol-induced tumour-suppressive miRNA expression and its anti-cancer activity are conserved among stilbene family members (Fig. 4e).

Discussion

Resveratrol exhibits strong anti-oxidant activity and is capable of inducing apoptosis in cancer cells. Therefore, resveratrol is believed to be efficacious at multiple carcinogenesis stages[4]. However, the underlying molecular mechanism of its anti-tumour activity has yet to be defined. In this study, we demonstrated that resveratrol up-regulated tumour-suppressive miRNAs, resulting in the induction of an anti-cancer effect against the CSC phenotype in cancer cells. We also demonstrated that resveratrol inhibited the invasiveness of breast cancer cells as one of the CSC phenotypes by activating miR-141 and miR-200c. However, the reason why resveratrol reduces the CSC population remains elusive. Recent studies have provided evidence that miR-200c strongly inhibits the ability of breast CSCs to form tumours *in vivo*[31]. These findings suggest that resveratrol shows multiple anti-cancer effects by reducing the CSC population through miR-200c activation.

Argonaute proteins are widely expressed and are involved in post-transcriptional gene silencing. Using microarrays to compare control and $Ago2^{-/-}$ cells, recent studies have demonstrated that Ago2 loss results in the global reduction of mature miRNAs in erythroblasts, fibroblasts, and hepatocytes[32]. However, it has not been determined whether Ago2 alterations can contribute to miRNA expression and the RNAi response. In this study, we show that Ago2 up-regulation by resveratrol leads to an increase in tumour-suppressive miRNAs and the enhancement of RNAi activity.

Pterostilbene has anti-diabetic properties and has been shown to be cytotoxic to a number of cancer cell lines *in vitro*[29,30]. Although pterostilbene and resveratrol have similar pharmacological properties, pterostilbene contains two methoxy groups and one hydroxyl group, while resveratrol has three hydroxyl groups (Supplementary Fig. 9). A recent study demonstrated that pterostilbene shows 95% bioavailability when orally administered, while resveratrol only has 20% bioavailability[33]. Furthermore, pterostilbene is a more powerful chemopreventive agent than resveratrol in colon cancer[34], showing that pterostilbene has several key advantages over resveratrol. In this study, we demonstrate that pterostilbene is more reliable than resveratrol in mediating the anti-cancer effect by inducing tumour-suppressive miRNAs and Ago2 expression. The reason for the difference in the anti-cancer activity of pterostilbene and resveratrol in cancer cells may be due to the expressed miRNAs.

It has been demonstrated that most tumours are characterised by globally diminished miRNA expression[16,17,35]. Thus, the delivery of tumour suppressive miRNAs may allow for the therapeutic restitution of physiological regulation programs lost in cancer and other disease states. However, miRNA therapy shares many of the disadvantages of other treatment approaches including delivery limitations and instability. Therefore, novel methods are required to resolve these issues. Based on this study, we hypothesise that the down-regulation of miRNAs in cancer cells is compensated by resveratrol, which induces the derepression of tumour suppressive miRNAs. Down-regulation of oncogenic miRNAs and up-regulation of tumour-suppressive miRNAs by resveratrol in prostate cancer cells has been reported[36]; however, the connection between resveratrol and the miRNA biogenesis machinery has not been investigated in detail. In this report, we demonstrated that resveratrol leads to a reduction in malignancy by not only activating tumour-suppressive miRNA transcription (Figs. 1d and 2b) but also enhancing the RNAi activity mediated by Ago2 induction (Figs. 2d, e, f and g). Our

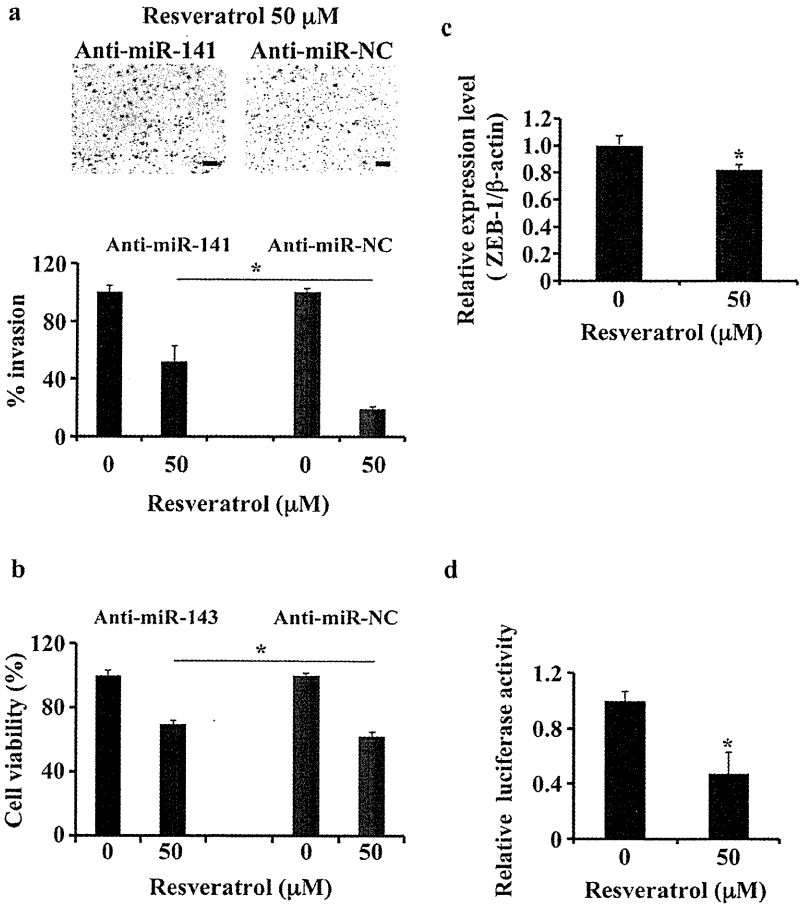

Figure 3 | Multiple anti-cancer effects of tumour-suppressive miRNAs induced by resveratrol. (a) MDA-MB231-luc-D3H2LN cells were grown and transiently transfected with anti-miR-141 or anti-miR-NC (control). After 4 hours, the cells were treated with resveratrol or DMSO (control) for 1 day and subjected to an invasion assay. Representative photographs (upper panel) and quantification (lower panel) are shown. Scale bar: 100 μm. (b) MDA-MB231-luc-D3H2LN cells were cultured and transiently transfected with anti-miR-143 or anti-miR-NC (control). After 4 hours, the cells were treated with resveratrol or DMSO (control) for 72 hours, and the cell viability was measured by the MTS assay. (c) MDA-MB231 cells were treated with resveratrol or DMSO (control). After 2 days of culture, the cell extract was subjected to real-time mRNA qRT-PCR. (d) MDA-MB231 cells were grown and transiently transfected with a ZEB-1 3′UTR or psiCheck2 vector (control) under resveratrol treatment. After 1 day of culture, the cells were subjected to a luciferase reporter assay. The values on the *y-axis* are depicted relative to the luciferase activity of cells treated with DMSO, which is defined as 1 (all data are shown as the mean ± s.e.m., *P<0.05).

demonstration that resveratrol potently suppresses even a severe and multifocal carcinogenesis model in the absence of measurable toxicity provides proof of the principle that miRNA replacement by resveratrol may be a clinically viable anti-cancer therapeutic strategy.

In conclusion, this study shows that an orally available small molecule can safely reduce many of the negative consequences at doses acceptable in humans with an overall improvement in health and survival. Our results raise the possibility that the regulation of tumour-suppressive miRNAs by natural agents could be a novel strategy in the design of combinational approaches using conventional therapies for tumour recurrence prevention and in achieving successful treatment outcomes in patients with cancer.

Methods

Reagents. Trans-resveratrol (98% purity) was purchased from Cayman Chemical, pterostilbene (98% purity) from Tokyo Chemical Industry, cycloheximide solution and 5, 6-dichlorobenzimidazole riboside from sigma, and docetaxel from Sanofi-Aventis. The antibiotic solution (containing 10,000 U/mL penicillin and 10 mg/mL streptomycin), the trypsin-EDTA mixture (containing 0.05% trypsin and EDTA), and FBS (fetal bovine serum) were obtained from Invitrogen. The FITC-conjugated anti-CD44 (clone L178) antibody was obtained from Becton Dickinson, and the APC- conjugated anti-CD24 (clone ML5) antibody, from Biolegend. The duplexes of each small interfering RNA (siRNA), targeting human Ago2 mRNA (siAgo2-1, GCACGGAAGUCCAUCUGAAUU, UUCAGAUGGACUUCCGUGCUU; siAgo2-2, GCAGGACAAAGAUGUAUUAUU, UAAUACAUCUUUGUCCUGCUU; siAgo2-3, GGGUCUGUGGUGAUAAAUAUU, UAUUUAUCACCACAGACCCUU; siAgo2-4, GUAUGAGAACCCAAUGUCAUU, UGACAUUGGGUUCUCAUACUU) and negative control 1 were purchased from Applied Biosystems[37].

Plasmids. The primary-miR-143 expression vector was purchased from TaKaRa BIO. The full-length human Ago2 cDNA was cloned into pIRES2-EGFP vector (Clontech). We amplified the upstream of human Ago2 gene (−1,770/−1 relative to the TSS) by PCR using human genomic DNA as template, and we cloned it into the pGL3-Basic vector. For the 3′UTR reporter plasmids, the nucleotides +3,399 to +3,953 of human ZEB1 cDNA were amplified and cloned downstream of the luciferase gene in the psiCHECK2 vector (Promega). For cloning the following primers were used for PCR: Ago2 promoter: 5′-ACGCGTATAGGGGATATGTGAAGGAGACA-3′ (forward) and 5′-CTCGAGATA CGCGCGCGCCACGGGCCCCG-3′ (reverse); ZEB1 3′UTR Fragment: 5′-ATAATACGCGTTAAAGGAAGCTGATTAATTAGATATGC-3′ (forward) and 5′-ATAATAAGCTTTTTGTAGTGCAGAAGTTCTCACATTTT-3′ (reverse)[22].

Cell culture. HEK293 cells (American Type Culture Collection) were cultured in Dulbecco's Modified Eagle's Medium containing 10% heat-inactivated FBS and an antibiotic-antimycotic (Invitrogen) at 37°C in 5% CO_2. MDA-MB-231 cells (American Type Culture Collection) and MDA-MB-231-luc-D3H2LN cells (Xenogen) were cultured in RPMI containing 10% heat-inactivated FBS and antibiotic-antimycotic at 37°C in 5% CO_2. Human mammary carcinoma cell lines, MCF7 cells and multidrug-resistant MCF7-ADR cells were provided by Shien-Lab,

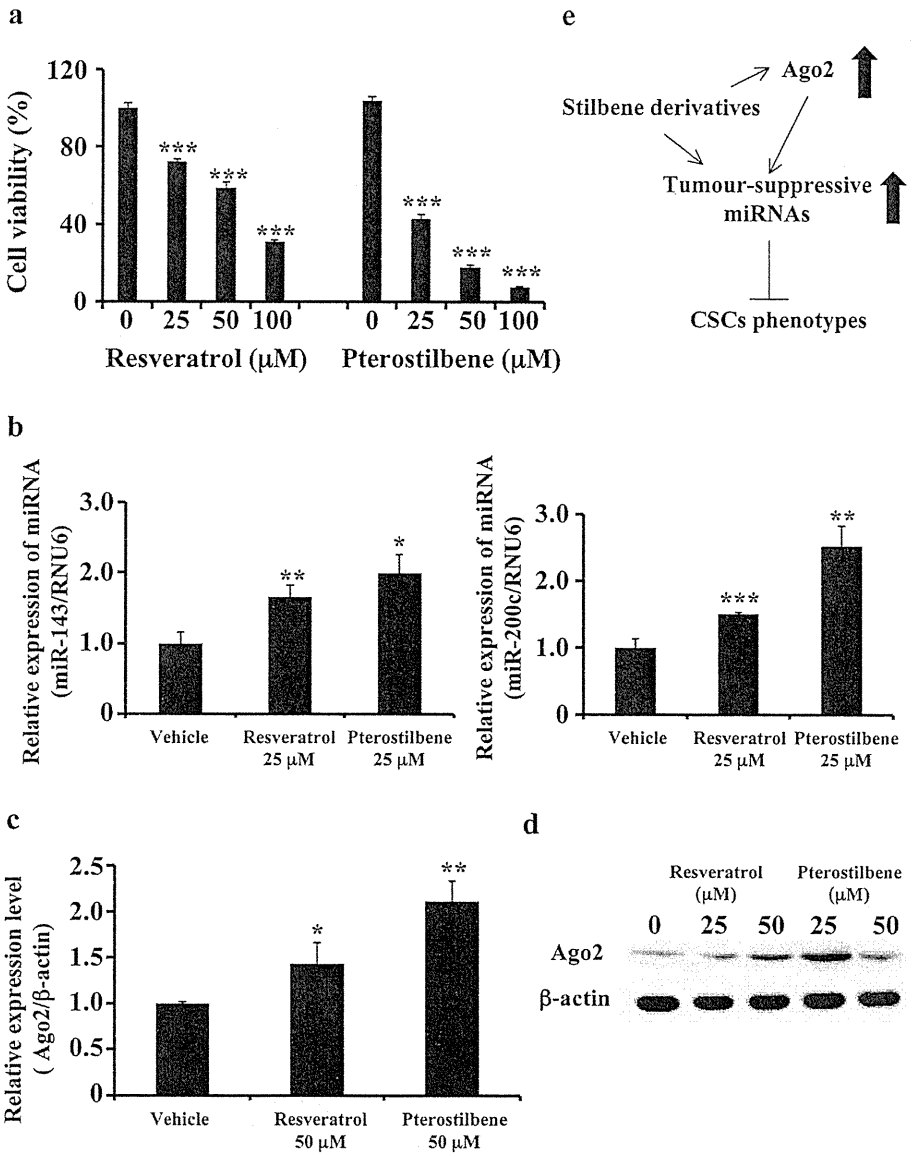

Figure 4 | Effects of pterostilbene on human breast cancer cells. (a) MDA-MB231-luc-D3H2LN cells were cultured in the presence or absence of resveratrol or pterostilbene at the indicated concentrations for 72 hours. Cell viability was measured using the MTS assay. The control wells were treated with DMSO. (b), (c) Expression levels of miR-143, miR-200c (b), and Ago2 (c) in MDA-MB231-luc-D3H2LN cells. The expression levels of the indicated miRNAs were examined in MDA-MB231-luc-D3H2LN cells 48 hours after treatment with pterostilbene. (d) MDA-MB231-luc-D3H2LN cells were treated with stilbenes for 72 hours, and Ago2 expression was detected by immunoblotting. Actin was used as a loading control. (e) Model of the regulation of tumour-suppressive miRNAs and Ago2 expression in the stilbene family (all data are shown as the mean ± s.e.m., *P<0.05, **P<0.01, ***P<0.001).

Medical Oncology, National Cancer Center Hospital of Japan. These cells were maintained in RPMI supplemented with 10% heat-inactivated FBS and antibiotic-antimycotic at 37°C in 5% CO_2. MCF10A cells, which were a spontaneously immortalized nontumorigenic epithelial cell line, (American Type Culture Collection) were maintained in an MEBM medium with 1% GA-1000, 50 μg/ml hydrocortisone, 1 μg/ml hEGF, 500 μg/ml insulin, and 4% BPE (Lonza) at 37°C in 5% CO_2.

Cell proliferation assay (MTS assay). Five thousand cells per well were seeded in 96-well plates. The following day, the cells were treated with resveratrol. After 3 days of culture, cell viability was measured using the Tetra Color One assay kit (Seikagaku Kohgyo) according to the instructions of the manufacturer. The absorbance at 450 nm was measured using Envision (Wallac).

Transwell invasion assay. Breast cancer cell invasion was assayed in 24-well Biocoat Matrigel invasion chambers (8 μm; Becton Dickinson) according to the manufacturer's protocol. Briefly, the cells were treated with resveratrol, and on the following day, 20,000 cells were plated in the upper chamber. The upper chamber contained resveratrol and the bottom chamber contained 10% FBS as a chemoattractant. Twenty-two hours later, the non-invasive cells were removed with a cotton swab. The cells that migrated through the membrane and stuck to the lower surface of the membrane were fixed with methanol and stained with Diff Quick staining. For quantification, the cells were counted under a microscope in four random fields. All assays were performed in triplicate. The data are expressed as the invasion percentage through the Matrigel matrix and membrane relative to migration through the control membrane according to the manufacturer's instructions.

Cell growth inhibition by cytotoxic agents and resveratrol. Breast cancer cells were plated as described above and allowed to attach overnight. The cultures were replenished with fresh medium containing 25 μM resveratrol for 24 hours and then exposed to 2.5 nM of the chemotherapeutic agent docetaxel for an additional 48 hours. Thus, for a single-agent treatment, the cells were exposed to resveratrol or docetaxel for 72 hours. The effect of resveratrol pretreatment on cell viability was examined by the MTS assay method.

Cell sorting and flow cytometric analysis. MDA-MB-231-luc-D3H2LN cells were treated with resveratrol. After culturing for 3 days, MDA-MB-231-luc-D3H2LN cells were suspended in their culture medium and subjected to a JSAN cell sorter (Bay Bioscience). At least one million cells were pelleted by centrifugation at 180 x *g* for 5 minutes at 4°C, resuspended in a 5-μL mixture of a monoclonal mouse anti-human CD44-FITC antibody (Becton Dickinson, clone L178) and a monoclonal mouse anti-human CD24-APC antibody (Biolegend, clone ML5), and incubated for 30 minutes at 4°C. Three independent experiments were performed.

Mammosphere assay. The CD44+/CD24− fraction from MDA-MB-231-luc-D3H2LN cells were resuspended in 1 : 1 DMEM/F12 (Invitrogen) basal medium freshly supplemented with 20 ng/mL human basic fibroblast growth factor (Invitrogen), 20 ng/mL epidermal growth factor (Invitrogen), 10 μg/mL heparin (Sigma-Aldrich), and 1 : 50 B27 supplement without vitamin A (Sigma-Aldrich) and seeded in 10-cm Ultra-Low Attachment Surface plates (Corning) at a density of 5000 cells. Ten days later, the plates were analysed for mammosphere formation.

Tumourigenicity assays in SCID hairless outbred mice. Six-week-old female SCID hairless outbred (SHO) mice were subcutaneously injected with 200 MDA-MB231-luc-D3H2LN cells in 25 μL of PBS and 25 μL of matrigel (n = 5). The mice were then treated with resveratrol (25 mg/kg/day) or ethanol (control) by intraperitoneal injection every day for 8 days. The tumour growth was monitored by injecting luciferin in the mice followed by measuring bioluminescence using an IVIS imaging system. The data were analysed using the LIVINGIMAGE 2.50 software (Xenogen). Six-week-old female SCID Hairless Outbred (SHO) mice were subcutaneously injected with 2000 MDA-MB231-luc-D3H2LN cells in 25 μL of PBS and 25 μL of Matrigel (n = 5). The mice were then treated with resveratrol (25 mg/kg) by intraperitoneal injection (IP) every day for 2 weeks and then with docetaxel (20 mg/kg) by intraperitoneal injection (IP) once per week for 2 weeks. The normalised fold changes (day 22 or day 29/day 15) of bioluminescence emitted from the whole body of the mice are shown. All experimental protocols involving animals were approved by the the Institute for Laboratory Animal Research, National Cancer Center Research Institute.

Isolation of microRNAs. Total RNAs were extracted from cultured cells using the QIAzol and miRNeasy Mini Kit (Qiagen) according to the manufacturer's protocol.

Quantitative Real-Time PCR (qRT-PCR). The qRT-PCR method has been previously described[38]. PCR was performed in 96-well plates using the 7300 Real-Time PCR System (Applied Biosystems). All reactions were performed in triplicate. All of the TaqMan microRNA assays were purchased from Applied Biosystems. hRNU6 was used as an invariant control. SYBR Green I qRT-PCR was performed, and the β-actin housekeeping gene was used to normalise the variation in the cDNA levels. The following pairs of primers were used for gene amplification: for pri-miR-16, 5′-GCAATTACAGTATTTTAAGAGATGAT-3′ (forward) and 5′- CAT-ACTCTACAGTTGTGTTTTAATGT-3′ (reverse); for pri-miR-141-200c, 5′-TGAGCTTGGGACTGCAGAG-3′ (forward) and 5′-CTGAGCCACCTTCCCC-TAC-3′ (reverse); for pri-miR-143, 5′-CAAGGTTTGGTCCTGGGTGCTCAAA-3′ (forward) and 5′-TGGTGGCCTGTGGCGGGACTCCAA-3′ (reverse); for ZEB1, 5′-AAGAATTCACAGTGGAGAGAAGCCA-3′ (forward) and 5′-CGTTTCTTGC-AGTTTGGGCATT-3′ (reverse); for E-cadherin, 5′-GTCCTGGGCAG-ACTGAATTT-3′ (forward) and 5′-GACCAAGAAATGGATCTGTGG-3′ (reverse); and for β-actin, 5′-GGCACCACCATGTACCCTG-3′ (forward) and 5′-CACGG-AGTACTTGCGCTCAG-3′ (reverse)[39].

Quantification of the Ago2 mRNA half-life. MDA-MB231-luc-D3H2LN cells were incubated with 5,6-dichlorobenzimidazole riboside (50 μM), which is an inhibitor of mRNA synthesis. The cells were then treated with 50 μM resveratrol and harvested at the indicated time points. Total cellular RNA was isolated using the RNeasy Mini kit (Qiagen). qRT-PCR analysis of Ago2 mRNA at each time point was performed as described above. The fold-change in the Ago2 mRNA abundance at each time point was determined by the following equation:

Fold change = $2^{-\Delta CT}$, where ΔCT = (CT, Ago2) target - (CT, Ago2) 0 h.

Transient transfection assays. The plasmid transfections were performed using Lipofectamine LTX (Invitrogen). The cell numbers and amount of plasmids for each transfection were determined according to the manufacturer's protocol. The transfection of siRNA and miRNA inhibitors was accomplished using the DharmaFECT transfection reagent (Thermo Scientific) according to the manufacturer's protocol.

Luciferase reporter assay. Cells were seeded in 96-well plates at 3000 cells per well the day before transfection. A total of 500 ng of Ago2 vector, 10 nM siRNA against luciferase and the AllStars negative control were added to each well. The cells were collected 1, 3, or 5 days after transfection and analysed using the Bright-Glo Luciferase Reporter Assay System (Promega).

Immunoblot analysis. SDS-PAGE gels were calibrated using Precision Plus protein standards (161-0375) (Bio-Rad), and anti-Ago2 (1 : 200) and anti-actin (1 : 1,000) were used as the primary antibodies. The dilution ratio of each antibody is indicated in parentheses. A peroxidase-labelled anti-mouse secondary antibody was used at a dilution of 1 : 10,000. Bound antibodies were visualised by chemiluminescence using the ECL Plus Western blotting detection system (RPN2132) (GE HealthCare), and luminescent images were analysed using a LuminoImager (LAS-3000; Fuji Film Inc.).

Quantification of Ago2 protein half-life. MDA-MB-231-luc-D3H2LN cells at 80% confluency were treated with 30 μg/ml cycloheximide (Sigma-Aldrich). The cells were then treated with 50 μM resveratrol and harvested at the indicated time points. The effect of resveratrol on Ago2 stability was examined by immunoblotting as reported above.

Statistical analysis. The data presented in bar graphs are the means ± s.e.m. of at least three independent experiments. Statistical analyses were performed using the Student's t-test.

1. Hartwell, J. L. & Schrecker, A. W. Components of Podophyllin. V. The Constitution of Podophyllotoxin1. *J Am Chem Soc* **73**, 2909–2916 (1951).
2. Baur, J. A. & Sinclair, D. A. Therapeutic potential of resveratrol: the in vivo evidence. *Nat Rev Drug Discov* **5**, 493–506 (2006).
3. Renaud, S. & de Lorgeril, M. Wine, alcohol, platelets, and the French paradox for coronary heart disease. *Lancet* **339**, 1523–1526 (1992).
4. Jang, M. *et al.* Cancer chemopreventive activity of resveratrol, a natural product derived from grapes. *Science* **275**, 218–220 (1997).
5. Fremont, L. Biological effects of resveratrol. *Life Sci* **66**, 663–673 (2000).
6. Hammell, C. M., Lubin, I., Boag, P. R., Blackwell, T. K. & Ambros, V. nhl-2 Modulates microRNA activity in Caenorhabditis elegans. *Cell* **136**, 926–938 (2009).
7. Stefani, G. & Slack, F. J. Small non-coding RNAs in animal development. *Nat Rev Mol Cell Biol* **9**, 219–230 (2008).
8. Kong, D. *et al.* miR-200 regulates PDGF-D-mediated epithelial-mesenchymal transition, adhesion, and invasion of prostate cancer cells. *Stem Cells* **27**, 1712–1721 (2009).
9. Zhao, J. J. *et al.* MicroRNA-221/222 negatively regulates estrogen receptor alpha and is associated with tamoxifen resistance in breast cancer. *J Biol Chem* **283**, 31079–31086 (2008).
10. Takeshita, F. *et al.* Systemic delivery of synthetic microRNA-16 inhibits the growth of metastatic prostate tumors via downregulation of multiple cell-cycle genes. *Mol Ther* **18**, 181–187 (2010).
11. Melkamu, T., Zhang, X., Tan, J., Zeng, Y. & Kassie, F. Alteration of microRNA expression in vinyl carbamate-induced mouse lung tumors and modulation by the chemopreventive agent indole-3-carbinol. *Carcinogenesis* **31**, 252–258 (2010).
12. Tsang, W. P. & Kwok, T. T. Epigallocatechin gallate up-regulation of miR-16 and induction of apoptosis in human cancer cells. *J Nutr Biochem* **21**, 140–146 (2010).
13. Li, Y. *et al.* Up-regulation of miR-200 and let-7 by natural agents leads to the reversal of epithelial-to-mesenchymal transition in gemcitabine-resistant pancreatic cancer cells. *Cancer Res* **69**, 6704–6712 (2009).
14. Sun, M. *et al.* Curcumin (diferuloylmethane) alters the expression profiles of microRNAs in human pancreatic cancer cells. *Mol Cancer Ther* **7**, 464–473 (2008).
15. Lee, H. P. *et al.* Dietary effects on breast-cancer risk in Singapore. *Lancet* **337**, 1197–1200 (1991).
16. Croce, C. M. Causes and consequences of microRNA dysregulation in cancer. *Nat Rev Genet* **10**, 704–714 (2009).
17. Gaur, A. *et al.* Characterization of microRNA expression levels and their biological correlates in human cancer cell lines. *Cancer Res* **67**, 2456–2468 (2007).
18. Al-Hajj, M., Wicha, M. S., Benito-Hernandez, A., Morrison, S. J. & Clarke, M. F. Prospective identification of tumorigenic breast cancer cells. *Proc Natl Acad Sci U S A* **100**, 3983–3988 (2003).
19. Al-Hajj, M. Cancer stem cells and oncology therapeutics. *Curr Opin Oncol* **19**, 61–64 (2007).
20. Al-Hajj, M., Becker, M. W., Wicha, M., Weissman, I. & Clarke, M. F. Therapeutic implications of cancer stem cells. *Curr Opin Genet Dev* **14**, 43–47 (2004).
21. Iorio, M. V. *et al.* MicroRNA gene expression deregulation in human breast cancer. *Cancer Res* **65**, 7065–7070 (2005).
22. Burk, U. *et al.* A reciprocal repression between ZEB1 and members of the miR-200 family promotes EMT and invasion in cancer cells. *EMBO Rep* **9**, 582–589 (2008).
23. Carmell, M. A. & Hannon, G. J. RNase III enzymes and the initiation of gene silencing. *Nat Struct Mol Biol* **11**, 214–218 (2004).
24. Kim, V. N. MicroRNA biogenesis: coordinated cropping and dicing. *Nat Rev Mol Cell Biol* **6**, 376–385 (2005).
25. Lingel, A., Simon, B., Izaurralde, E. & Sattler, M. Structure and nucleic-acid binding of the Drosophila Argonaute 2 PAZ domain. *Nature* **426**, 465–469 (2003).
26. Korpal, M., Lee, E. S., Hu, G. & Kang, Y. The miR-200 family inhibits epithelial-mesenchymal transition and cancer cell migration by direct targeting of E-cadherin transcriptional repressors ZEB1 and ZEB2. *J Biol Chem* **283**, 14910–14914 (2008).
27. Xu, B. *et al.* miR-143 decreases prostate cancer cells proliferation and migration and enhances their sensitivity to docetaxel through suppression of KRAS. *Mol Cell Biochem* **350**, 207–213 (2011).
28. Burk, U. *et al.* A reciprocal repression between ZEB1 and members of the miR-200 family promotes EMT and invasion in cancer cells. *Embo Reports* **9**, 582–589 (2008).

29. Rimando, A. M. *et al.* Cancer chemopreventive and antioxidant activities of pterostilbene, a naturally occurring analogue of resveratrol. *J Agric Food Chem* **50**, 3453–3457 (2002).
30. Stivala, L. A. *et al.* Specific structural determinants are responsible for the antioxidant activity and the cell cycle effects of resveratrol. *J Biol Chem* **276**, 22586–22594 (2001).
31. Shimono, Y. *et al.* Downregulation of miRNA-200c links breast cancer stem cells with normal stem cells. *Cell* **138**, 592–603 (2009).
32. O'Carroll, D. *et al.* A Slicer-independent role for Argonaute 2 in hematopoiesis and the microRNA pathway. *Genes Dev* **21**, 1999–2004 (2007).
33. Kapetanovic, I. M., Muzzio, M., Huang, Z., Thompson, T. N. & McCormick, D. L. Pharmacokinetics, oral bioavailability, and metabolic profile of resveratrol and its dimethylether analog, pterostilbene, in rats. *Cancer Chemother Pharmacol* (2010).
34. Chiou, Y. S. *et al.* Pterostilbene is more potent than resveratrol in preventing azoxymethane (AOM)-induced colon tumorigenesis via activation of the NF-E2-related factor 2 (Nrf2)-mediated antioxidant signaling pathway. *J Agric Food Chem* **59**, 2725–2733 (2011).
35. Chang, T. C. *et al.* Transactivation of miR-34a by p53 broadly influences gene expression and promotes apoptosis. *Mol Cell* **26**, 745–752 (2007).
36. Dhar, S., Hicks, C. & Levenson, A. S. Resveratrol and prostate cancer: Promising role for microRNAs. *Mol Nutr Food Res* **55**, 1219–1229 (2011).
37. Meister, G. *et al.* Human Argonaute2 mediates RNA cleavage targeted by miRNAs and siRNAs. *Mol Cell* **15**, 185–197 (2004).
38. Mitchell, P. S. *et al.* Circulating microRNAs as stable blood-based markers for cancer detection. *Proc Natl Acad Sci U S A* **105**, 10513–10518 (2008).
39. Suzuki, H. I. *et al.* Modulation of microRNA processing by p53. *Nature* **460**, 529–533 (2009).

Acknowledgements

This work was supported in part by a Grant-in-Aid for the Third-Term Comprehensive 10-Year Strategy for Cancer Control, a Grant-in-Aid for Scientific Research on Priority Areas Cancer from the Ministry of Education, Culture, Sports, Science and Technology, the National Cancer Center Research and Development Fund, the Program for Promotion of Fundamental Studies in Health Sciences of the National Institute of Biomedical Innovation (NiBio), Project for Development of Innovative Research on Cancer Therapeutics, and the Japan Society for the Promotion of Science (JSPS) through the "Funding Program for World-Leading Innovative R&D on Science and Technology (FIRST Program)" initiated by the Council for Science and Technology Policy (CSTP). We thank Ayako Inoue for excellent technical assistance. We thank Dr.Izuho Hatada for providing the information about Ago2 promoter region.

Author contributions

TO supervised the project. KH performed a significant amount of the experimental work. TO, KH, NK, and YY wrote the manuscript and prepared the figures and tables. *In vivo* experiments were carried out by KH, NK, YY, RT, and FT.

Additional information

Supplementary information accompanies this paper at http://www.nature.com/scientificreports

Competing financial interests: The authors declare no competing financial interests.

How to cite this article: Hagiwara, K. *et al.* Stilbene derivatives promote Ago2-dependent tumour-suppressive microRNA activity. *Sci. Rep.* **2**, 314; DOI:10.1038/srep00314 (2012).

Inhibition of Stabilin-2 elevates circulating hyaluronic acid levels and prevents tumor metastasis

Yoshikazu Hirose[a,1], Eiko Saijou[a,1], Yasuyoshi Sugano[a,1], Fumitaka Takeshita[b], Satoshi Nishimura[c,d], Hidenori Nonaka[a], Yen-Rong Chen[a], Keisuke Sekine[a], Taketomo Kido[a], Takashi Nakamura[e], Shigeaki Kato[e], Toru Kanke[f], Koji Nakamura[f], Ryozo Nagai[c,d,g], Takahiro Ochiya[b], and Atsushi Miyajima[a,2]

[a]Laboratory of Cell Growth and Differentiation and [e]Laboratory of Nuclear Signaling, Institute of Molecular and Cellular Biosciences, University of Tokyo, Tokyo 113-0032, Japan; [b]Division of Molecular and Cellular Medicine, National Cancer Center Research Institute, Tokyo 104-0045, Japan; [c]Department of Cardiovascular Medicine, [d]Translational Systems Biology and Medicine Initiative, and [g]Global Center of Excellence Program, Comprehensive Center of Education and Research for Chemical Biology of the Diseases, University of Tokyo, Tokyo 113-8655, Japan; and [f]LivTech Inc., Kanagawa 216-0001, Japan

Edited by Joan Massagué, Memorial Sloan-Kettering Cancer Center, New York, NY, and approved February 3, 2012 (received for review October 31, 2011)

Hyaluronic acid (HA) has been implicated in the proliferation and metastasis of tumor cells. However, most previous studies were conducted on extracellular matrix or pericellular HA, and the role of circulating HA in vivo has not been studied. HA is rapidly cleared from the bloodstream. The scavenger receptor Stabilin-2 (Stab2) is considered a major clearance receptor for HA. Here we report a dramatic elevation in circulating HA levels in Stab2-deficient mice without any overt phenotype. Surprisingly, the metastasis of B16F10 melanoma cells to the lungs was markedly suppressed in the Stab2-deficient mice, whereas cell proliferation was not affected. Furthermore, administration of an anti-Stab2 antibody in Stab2$^+$ mice elevated serum HA levels and prevented the metastasis of melanoma to the lung, and also suppressed spontaneous metastasis of mammary tumor and human breast tumor cells inoculated in the mammary gland. Administration of the antibody or high-dose HA in mice blocked the lodging of melanoma cells to the lungs. Furthermore, HA at high concentrations inhibited the rolling/tethering of B16 cells to lung endothelial cells. These results suggest that blocking Stab2 function prevents tumor metastasis by elevating circulating HA levels. Stab2 may be a potential target in antitumor therapy.

cancer | hyaluronan | imaging | antibody therapy | sinusoid

Scavenger receptors mediate the endocytosis of metabolic waste products produced under normal and pathological conditions, as well as harmful foreign substances, such as bacterial debris absorbed in the gut. The liver functions as a major filter to eliminate such molecules from the circulation. Liver-specific capillaries known as sinusoids are vital to this function; for example, more than 90% of circulating hyaluronic acid (HA) is cleared by liver sinusoids (1). Sinusoidal walls consist of hepatic sinusoid endothelial cells (HSECs), stellate cells, and liver resident macrophages known as Kupffer cells. HSECs and Kupffer cells express various types of scavenger receptors to fulfill the filter functions. Among those scavenger receptors, Stabilin-1 (Stab1, also known as FEEL-1 and CLEVER-1) and Stabilin-2 (Stab2, also known as FEEL-2 and HARE) are structurally related, exhibiting 55% homology at the protein level, and expressed on HSECs (2).

Stab1 and Stab2 are large type I transmembrane glycoproteins containing four domains with EGF-like repeats, seven fasciclin-1 domains, and an X-link domain (3). Despite these two glycoproteins' structural similarity, the spectrum of their ligands differs significantly. Stab1 is expressed on lymphatic vessels and macrophages as well as HSEC and binds to acetylated low-density lipoprotein (ac-LDL), secreted protein acidic and rich in cysteine, placental lactogen, growth differentiation factor 15, and Gram-positive and Gram-negative bacteria, but not to HA (2, 4–8). It also mediates leukocyte trafficking (9). Stab2 is expressed on the sinusoid endothelium in the liver, spleen, and lymph nodes and has been used as a specific marker for HSECs (10). It binds to and mediates the endocytosis of HA, advanced glycation end products-modified protein, and heparin in addition to ac-LDL, growth differentiation factor 15, and bacteria (2, 4). Stab2 also recognizes membrane phosphatidylserine of apoptotic cells (11). Previous studies found that unlabeled chondroitin sulfate inhibited the uptake of ^{125}-I-HA (12), and that ac-LDL binding to Stab2 was partially competed by heparin and dextran sulfate, but not competed by HA (13). These findings suggest that the HA binding site overlaps with the binding site of chondroitin sulfate but differs from the binding sites of ac-LDL, heparin, and dextran sulfate.

HA is a glycosaminoglycan of the extracellular matrix consisting of tandem repeats of D-glucuronic acid and *N*-acety-D-glucosamine. HA is abundant in the umbilical cord, articular joints, cartilage, and vitreous humor (14). It has been implicated in various physiological functions, including lubrication, water homeostasis, filtering effects, regulation of plasma protein distribution, angiogenesis, wound healing, and chondrogenesis (15). Signal transduction and functions of HA differ depending on molecular size; for example, high molecular weight HA suppresses angiogenesis, whereas HA fragments stimulate angiogenesis (16).

HA interacts with various cell surface receptors, including CD44, Lyve-1, TLRs, RHAMM, and Stab2 (17, 18). CD44, the most extensively characterized of these receptors, is expressed at varying levels in most immune cells and is involved in their rolling and extravasation via HA displayed on endothelial cells (ECs) (19). CD44 is also implicated in tumorigenesis and a marker for cancer stem cells (reviewed in ref. 20). Lyve-1 is structurally related to CD44 and is expressed in lymphatic vessels as well as in HSECs (21). TLR2 and TLR4 bind to HA or a complex of HA and HA-binding protein (18, 22); however, none of the mice deficient for CD44, Lyve-1, or TLRs have been shown to affect circulating HA levels in vivo. Although Stab1 and Stab2 are structurally related scavenger receptors with the HA-binding link domain, only Stab2 binds HA, and thus it has been considered the primary scanvenger receptor for HA (2, 3, 5).

HA, HA synthases (HAS), hyaluronidases, and HA receptors have been implicated in various tumors, including carcinomas, lymphomas, and melanocytic and neuronal tumors (23, 24). Overexpression and knockdown of HAS and hyaluronidases

Author contributions: Y.H., E.S., Y.S., H.N., and A.M. designed research; Y.H., E.S., Y.S., F.T., S.N., Y.-R.C., K.S., T. Kido, T.N., S.K., T. Kanke, K.N., R.N., and T.O. performed research; Y.H., E.S., Y.S., F.T., S.N., and A.M. analyzed data; and Y.H., E.S., and A.M. wrote the paper.

The authors declare no conflict of interest.

This article is a PNAS Direct Submission.

[1]Y.H., E.S., and Y.S. contributed equally to this work.

[2]To whom correspondence should be addressed. E-mail: miyajima@iam.u-tokyo.ac.jp.

This article contains supporting information online at www.pnas.org/lookup/suppl/doi:10.1073/pnas.1117560109/-/DCSupplemental.

have revealed that HA positively regulates proliferation, invasion, cell motility, multidrug resistance, and epithelial–mesenchymal transition in many tumor cell lines in vitro and in vivo (reviewed in ref. 23). Furthermore, an HAS inhibitor, 4-methylubelliferon, has been shown to decrease tumor proliferation and metastasis (25, 26).

Despite the importance of HA in tumorigenesis, assessing the role of circulating HA in tumor progression is difficult, because HA administered in the body is rapidly eliminated from the bloodstream (1). In this study, we generated Stab2 KO mice in which plasma HA levels were significantly elevated without any overt phenotype. Unexpectedly, tumor metastasis was markedly suppressed in these mice. We also found that administration of an anti-Stab2 antibody in WT mice elevated circulating HA levels and prevented tumor metastasis. Finally, we found that administration of a high dose of HA prevented the attachment of melanoma cells to the lungs in vivo and in vitro, and examined a possible link between circulating HA levels and tumor metastasis.

Results

Elevation of Circulating HA Levels in Stab2 KO Mice. To address the physiological roles of Stab2 in vivo, we generated a Stab2 KO mouse line by replacing most of the first exon, including the ATG initiation codon and the first intron, with the LacZ and neomycin resistance genes (Figs. S1 *A–C*). The lack of Stab2 expression in KO mice was confirmed by RT-PCR and immunostaining (Figs. S1 *D* and *H* and S2*D*), Stab2-deficient mice were born according to the Mendelian ratio, grew normally, and showed no apparent abnormalities (Fig. S1 *E* and *F*). Histological analyses revealed no significant changes (Fig. S1*G*). Staining of liver sections with the anti-CD31 antibody, which binds HSECs as well as other types of ECs in the liver, demonstrated normal development of HSECs (Fig. S1*H*). Furthermore, we found no significant differences in conventional diagnostic markers for functions of the pancreas, liver, and kidney (Table S1). These results indicate that Stab2 is dispensable for normal development and viability in mice.

Given that Stab2 is a known scavenger receptor that binds and eliminates from the circulation various substances, including HA, ac-LDL, and heparin (4, 27, 28), we assessed the circulating levels of these substances in Stab2 KO mice. Although serum levels of ac-LDL and heparin were unchanged in the Stab2 KO mice (Table S1), serum HA levels were dramatically increased, by as much as 59-fold over control values (Fig. 1*A*). Because HA's molecular size affects its function (16), we next analyzed the molecular size of serum HA by electrophoresis using Stains-All (which stains negatively charged molecules), and estimated it as ~40 kDa (Fig. S1*J*). Given that >90% of the circulating HA is cleared by HSECs (1), and that Stab2 is specifically expressed in HSECs, we examined whether the high serum HA levels in Stab2 KO mice were due to impaired endocytosis. We prepared HSECs from WT and Stab2 KO mice and quantitatively evaluated their endocytotic activity based on the internalization of FITC-labeled HA and DiI-labeled ac-LDL (DiI-Ac-LDL) (Fig. 1*B* and *C* and Fig. S1 *K* and *L*). Although there was no significant difference in the internalization of DiI-Ac-LDL between WT and Stab2 KO mice, the internalization of HA into Stab2-deficient HSECs was markedly decreased, to only ~8% of the WT level. We also examined the expression of other HA receptors (CD44 and Lyve-1) and HA synthases (HAS1, HAS2, and HAS3) that can potentially affect HA levels, but found no significant changes in the Stab2 KO mice (Fig. S2 *A* and *B*). These results provide clear evidence that Stab2 is the major clearance receptor for HA in the body.

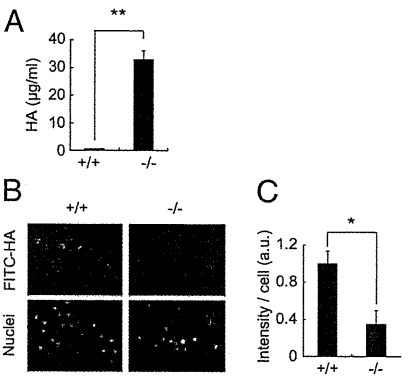

Fig. 1. Serum HA levels and internalization of HA in Stab2-deficient cells. (*A*) Serum HA levels in WT ($^{+/+}$) and homozygous ($^{-/-}$) littermates ($n = 3$; $^{**}P < 0.01$). (*B*) Internalization of FITC-HA in Percoll-purified HSECs from Stab2$^{+/+}$ and Stab2$^{-/-}$ littermates. (*Upper*) Fluorescence of FITC-HA incorporated into cells. (*Lower*) Hoechst 33342 staining. (*C*) Quantification of FITC fluorescence intensity ($n = 4$; $^{*}P < 0.05$).

Metastasis of Melanoma Cells Is Suppressed in Stab2 KO Mice. The elevation in serum HA levels in Stab2 KO mice prompted us to examine whether the lack of Stab2 has any effects on tumorigenesis. B16 melanoma cells are known to form tumor nodules in the lung when injected i.v. We administered B16F10 cells i.v. in littermates of Stab2$^{+/+}$ and Stab2$^{-/-}$ mice. After 14 d, numerous black nodules had formed on the lung surfaces of the Stab2$^{+/+}$ mice, but surprisingly, nodular formation was markedly reduced in Stab2$^{-/-}$ mice (Fig. 2 *A* and *B*). In contrast, tumor formation resulting from the s.c. inoculation of melanoma cells did not differ significantly between the Stab2$^{+/+}$ and Stab2$^{-/-}$ mice (Fig. 2*C*). Moreover, our in vitro experiments showed that the proliferation of B16F10 cells was not affected by HA, and a cell cycle analysis of B16F10 cells recovered from lung tumors revealed no difference between the Stab2 KO and WT mice (Fig. S3*A*). These results indicate that the metastasis, but not the proliferation, of melanoma cells was affected by the lack of Stab2.

To analyze the early stages of metastasis, we also conducted imaging in vivo, because the nodules of B16F10 cells at day 7 were too small to count. B16F10 cells were stably transfected with the firefly luciferase gene to generate B16F10-luc-G5 cells,

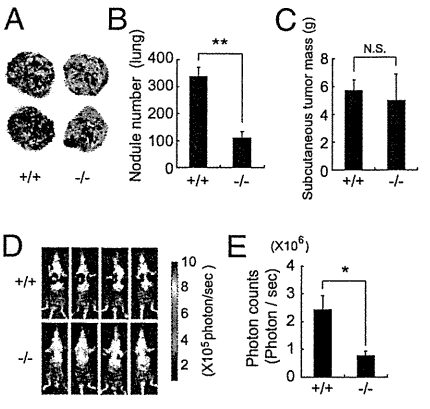

Fig. 2. Homing of B16F10 melanoma to the lungs in Stab2 KO mice. B16F10 cells (5×10^5) were injected via the tail vein in Stab2$^{+/+}$ and Stab2$^{-/-}$ littermates. (*A*) Metastatic nodules formed on the lungs at day 14 after the injection. (*B*) Numbers of nodules formed on the lungs were counted manually ($^{+/+}$, $n = 9$; $^{-/-}$, $n = 6$; $^{**}P < 0.01$). (*C*) Size of tumors formed by s.c. inoculated melanoma cells at day 21 [$^{+/+}$, $n = 8$; $^{-/-}$, $n = 6$; $^{*}P > 0.05$ (not significant)]. (*D*) Metastasis of i.v. injected B16F10-luc-G5 cells measured by luminescence using IVIS in vivo imaging at day 7. (*E*) Quantification of photon counts in *C* ($^{+/+}$, $n = 6$; $^{-/-}$, $n = 5$; $^{*}P < 0.05$).

which were then injected i.v. into littermates of Stab2$^{+/+}$ and Stab2$^{-/-}$ mice. After 7 d, tumor metastasis was measured based on the luminescence of luciferase. Photon counts were significantly decreased in the Stab2$^{-/-}$ mice, indicating inhibition of metastasis at an early stage (Fig. 2 *D* and *E*).

Administration of Anti-Stab2 Antibody Increases Serum HA Levels and Prevents Tumor Metastasis. We next investigated whether Stab2 functions could be blocked by an anti-Stab2 antibody in vivo. We generated several mAbs against the extracellular domain of Stab2 by immunizing rats with BaF3 cells expressing Stab2 and one of them (#34-2, ref. 10) was found to inhibit HA binding to Stab2 as assessing by internalization of FITC-labeled HSECs in vitro (Fig. 3*A*). To test whether that anti-Stab2 mAb has any effect on the plasma HA level in vivo, we injected it i.p. into C57BL/6 mice every 3 d and monitored serum HA levels. Within 3 d of the first injection, serum HA levels were increased in all of the mice given the anti-Stab2 mAb, but not in the mice treated with rat IgG (Fig. 3*B*). We obtained the same results using SCID mice (Fig. 4 *A* and *J*). These findings clearly indicate that the anti-Stab2 mAb effectively increased plasma HA levels by inhibiting Stab2 function in vivo. To examine whether this mAb prevents tumor metastasis, we injected mice with either anti-Stab2 mAb or control rat IgG, followed 2 d later by i.v. injection of B16F10 cells. The anti-Stab2 mAb significantly suppressed metastasis (Fig. 3 *C* and *D*). Taken together, these results indicate that the anti-Stab2 mAb elevates circulating HA levels by blocking the clearance of HA in HSECs, and that serum HA levels are inversely correlated with tumor metastasis.

Because the anti-Stab2 mAb elevated plasma HA levels in immune deficient mice, we investigated its effect on spontaneous metastasis by multiple cancer cells in SCID mice. To do so, we transplanted MDA-MB-231-luc-D3H2LN cells (human mammary gland adenocarcinoma cells expressing luciferase) into the abdominal mammary glands of SCID mice. After 21 d, tumor metastasis in the upper body, including the brachial lymph nodes, was evaluated by luminescence analysis. The number of photons derived from metastasized cells in the upper body was significantly reduced in the mice treated with the anti-Stab2 mAb (Fig. 4*A–D*). We also transplanted 4T1-LucNeo-1H mouse mammary tumor cells expressing luciferase into the mammary fad pads of the mice. Starting at 2 d after tumor injection, each animal was given either anti-Stab2 mAb or rat IgG every 3 d. At 3 wk after the start of antibody treatment, metastatic luminescence signals and the numbers of histological lesions in the lung were reduced in the anti-Stab2 mAb-treated mice. Given the lack of significant difference in the size of primary tumors (Fig. 4 *E–L*), anti-Stab2 mAb can be considered to inhibit spontaneous metastasis.

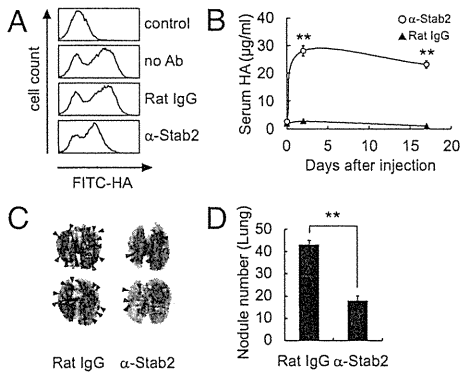

Fig. 3. Inhibition of HA clearance and metastasis by anti-Stab2 mAb. (*A*) HSECs were incubated with anti-Stab2 mAb or rat IgG, and the cell internalization of FITC-HA was analyzed by flow cytometry. (*B*) Anti-Stab2 mAb or rat IgG (3 mg/kg body weight) was administered i.p. to C57BL/6 mice on days 0, 3, and 17, and serum HA levels were measured ($n = 5$; $^{**}P < 0.01$). (*C*) At 2 d after the i.p. administration of anti-Stab2 mAb or control IgG, 5×10^4 B16F10 cells were injected i.v. via the tail vein. Anti-Stab2 mAb or control IgG was administered every 3 d. The lungs at 14 d are shown. Arrowheads indicate nodules of B16F10 cells. (*D*) The number of nodules formed on the lungs were counted manually ($n = 10$; $^{**}P < 0.01$). α-Stab2 denotes anti-Stab2 mAb.

Examination of Possible Mechanisms for Inhibition of Metastasis. To investigate the inhibitory mechanism of metastasis observed in the Stab2 KO and anti-Stab2 mAb-treated mice, we first analyzed whether HA affects tumor cells in vitro. We evaluated the effects of a 31-kDa HA (similar in size to HA in circulation; Fig. S1*J*), on cell proliferation, apoptosis induced by hydrogen peroxide, migration, and invasion into the basal membrane. None of these assays demonstrated any significant effect of HA on tumor cells at various concentrations (Fig. S3 *A–E*).

Because the proliferation as well as metastasis of tumors is under surveillance by the immune system, and HA has been implicated in the immune system, we examined the immune cells of Stab2 KO mice for any changes. We found no significant differences in fractions of regulatory T cells, NK cells, macrophages, and myeloid-derived suppressor cells in bone marrow, peripheral blood, and spleen in Stab2 KO mice compared with WT mice (Fig. S4*A*). In addition, we found no alterations in serum levels of TNF-α, IFN-γ, IL-2, IL-4, IL-6 IL-10, and IL-17A (Fig. S4*B*), or in the activation of macrophages in vivo and sensitivity to i.p. LPS (Figs. S2*E* and S4*C*). These results showing no significant alterations in the immune system in Stab2 KO mice suggest that the immune system may not be directly involved in the inhibition of tumor metastasis.

Attachment of Melanoma Cells to the Lungs Is Prevented by an Increase in Plasma HA. Intravenously injected melanoma cells are thought to roll through the bloodstream and lodge in the lungs, where they proliferate. Our finding that the melanoma cells injected s.c. in Stab2 KO mice formed tumors as large as those seen in their WT littermates (Fig. 2*C*) suggests that the homing of i.v. injected tumor cells to the lungs might be altered in the mutant mice. To analyze the attachment of melanoma cells to the lung in vivo, we inoculated B16F10-luc-G5 cells i.v. After 6 h, mice were perfused with PBS via the portal vein to remove blood cells from the tissues, and luciferase activity in the lungs was evaluated. The luciferase activity in the lungs was significantly decreased in Stab2 KO mice and in mice treated with the anti-Stab2 mAb compared with WT mice and rat IgG-treated mice (Fig. 5 *A* and *B*). These results indicate that tumor metastasis was prevented at an early stage of penetration in the lungs.

Because plasma HA level has been suggested to be involved in the metastasis of melanoma cells, and HA binds to cell surface molecules such as CD44, we investigated whether HA mediates the attachment of tumor cells to tissues. We first tested the binding of melanoma cells to HA by plating B16F10 cells on an HA-coated plate, and found that the cells attached to the plate via HA (Fig. S3*F*). Adding HA at the concentration found in Stab2 KO mouse sera inhibited the binding of B16F10 to the HA-coated plate. This finding suggests that the increased plasma HA in the mutant mice inhibits metastasis by preventing the attachment of melanoma cells to the lung via HA.

We also investigated whether HA prevents the attachment of B16F10 cells to the lung. Although i.v. injected HA is rapidly cleared from the bloodstream (1), we found that a very high dose of HA administered via the tail vain elevated the serum HA level for several hours (Fig. 5*C*). Thus, we injected HA at a dose of 20 mg/kg body weight every 8 h for 24 h to increase the plasma HA level, and then transplanted B16F10-luc-G5 cells. At 6 h after B16F10-luc-G5 cell transplantation, luciferase activity in the lungs was significantly reduced, whereas the serum

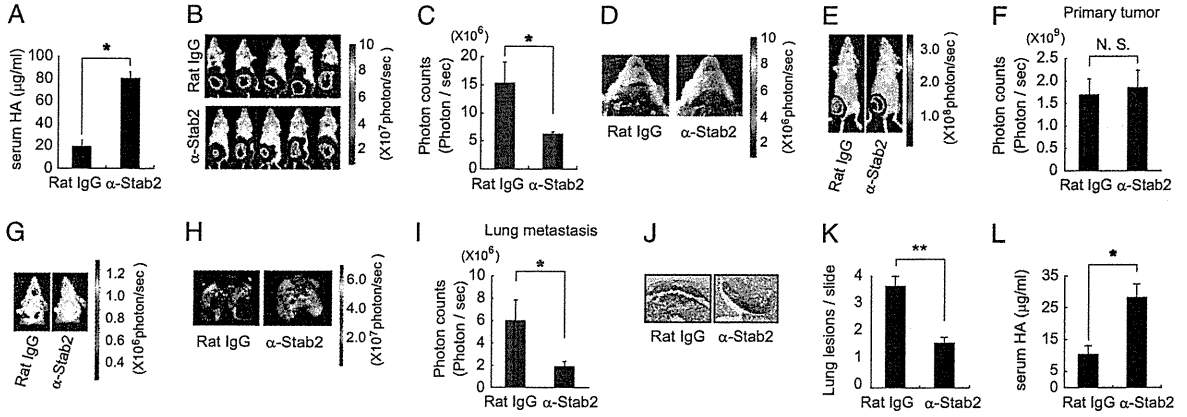

Fig. 4. Anti-Stab2 antibody prevents spontaneous metastasis of human and mouse mammary tumor cells in SCID mice. (*A*) SCID mice were i.p. injected with anti-Stab2 mAb or rat IgG (3 mg/kg), and serum HA levels were measured at 7 d after the injection ($n = 5$; $^*P < 0.05$). (*B*) MDA-MB-231-luc-D3H2LN cells were grafted in the mammary gland of SCID mice injected i.p. with anti-Stab2 mAb or control IgG (3 mg/kg). Luminescence was measured by IVIS at day 21. (*C*) Quantification of photon counts in the upper body at day 21 ($n = 5$; $^*P < 0.05$). (*D*) Luminescence of the opened thorax in *B*. (*E*) Mouse 4T1-LucNeo-1H mammary tumor cells were grafted into a mammary fat pad of the mice. At 2 d after tumor injection, each animal was given anti-Stab2 mAb or Rat IgG i.p. every 3 d, for a total of seven injections. Luminescence of primary tumors was measured by IVIS at day 21. (*G*) For the detection of signals from metastatic regions, the lower part of each animal was shielded with black paper before reimaging, to minimize bioliminescence from primary tumor. At the end of the experiment (day 21), ex vivo imaging was performed on collected lungs. Control group mice exhibited spontaneous lung metastasis. (*F*, *H*, and *I*) Quantification of bioluminescence emitted from primary tumors on mice and lung metastatic regions at the end of the experiment. Data represent mean ± SD ($n = 4$; $^*P < 0.05$ vs. other groups). (*J*) H&E-stained sections of spontaneous lung metastasis lesions at day 21. (*K*) Quantification of lung lesions in *J*. Data represent mean values ($n = 32$; $^{**}P < 0.01$ vs. other groups). (*L*) Serum HA levels measured at the end of the experiment ($n = 4$; $^*P < 0.05$). α-Stab2 denotes anti-Stab2 mAb.

HA level remained elevated in those mice pretreated with HA (Fig. 5 *D* and *E*).

Finally, to prove that increased HA level decreases the arrest of tumor cells in lung capillaries, we performed in vitro rolling/tethering assays using a VenaEC system. Pulmonary ECs from WT mice were cultured on VenaEC substrates and connected to a microfluidic device. Rolling/tethering between pulmonary cells and B16 melanoma cells under share stress was observed (Fig. 5*F*). At a low HA concentration (0.55 μg/mL, similar to $Stab2^{+/+}$ serum levels), B16 melanoma cells were tethered to pulmonary

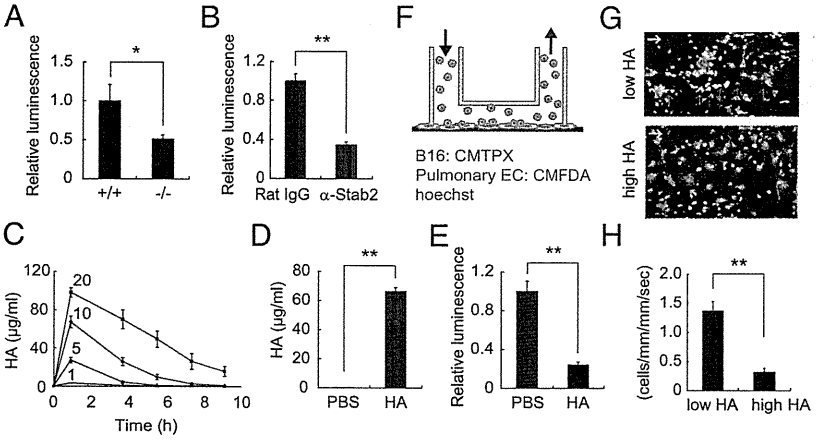

Fig. 5. HA inhibits attachment of B16F10 cells. (*A*) B16F10-luc-G5 cells (1.5×10^6) were injected into the tail vein of $Stab2^{+/+}$ and $Stab2^{-/-}$ mice, and 6 h later, the mice were perfused with PBS via the portal vein to remove blood cells from tissues. The B16F10-luc-G5 cells remaining in the lungs were detected by luciferase analysis ($^{+/+}$, $n = 6$; $^{-/-}$, $n = 7$; $^*P < 0.05$). (*B*) At 2 d after the i.p. administration of anti-Stab2 or rat IgG, B16F10-luc-G5 cells (1.5×10^6) were injected into the tail vein. At 6 h later, the injection cells remaining in the lungs were detected by luciferase analysis as in *A* (rat IgG, $n = 5$; $^{-/-}$, $n = 6$; $^{**}P < 0.01$). (*C*) HA at doses of 1, 5, 10, and 20 mg/kg was injected i.v., and serum HA levels were measured serially ($n = 4$). (*D*) HA at 20 mg/kg or an equal volume of PBS was injected i.v. every 8 h. At 24 h after the first HA injection, B16F10-luc-G5 cells (1.5×10^6) were injected into the tail vein with 20 mg/kg of HA. After 6 h, serum samples were collected, and plasma HA levels were analyzed at the end of experiment ($n = 8$; $^{**}P < 0.01$). (*E*) Cells remaining in the lungs were detected based on luciferase activity at *D* as in *A* ($n = 8$; $^{**}P < 0.01$). (*F*) Schematic diagram of the VenaEC system (Cellix). (*G*) Rolling and/or tethering of B16 melanoma cells onto pulmonary ECs using the VenaEC system. Pulmonary ECs from 6-d-old WT (C57BL/6) mice were isolated, cultured, and stained with 5 μM CMFDA (green) and 10 μM Hoechst 33342 (blue). B16F10 cells were stained with 5 μM CMTPX (red) and 10 μM Hoechst (blue). The pulmonary cell chamber was connected to a microfluidic device, and perfusion for 5 min with VL medium containing stained B16F10 cells at 0.7 dynes/cm^2 was performed during confocal observation of cell kinetics. Representative images of B16 melanoma cells with low (0.55 μg/mL) and high (33 μg/mL) HA concentrations are shown (Movies S1 and S2). White arrows denote flow directions, and red arrows indicate rolling and/or tethering B16F10 cells. (*H*) Quantification of rolling/tethering to the pulmonary ECs. The numbers of rolling/ tethering B16F10 cells were counted. Note that HA at high concentrations inhibited the rolling/tethering of melanoma cells onto pulmonary endothelium ($n = 20$ images from five experiments; $^*P < 0.05$). (Scale bar: 100 μm.) α-Stab2 denotes anti-Stab2 mAb.